A dispensable paralog of succinate dehydrogenase subunit C mediates standing resistance towards a subclass of SDHI fungicides in *Zymoseptoria tritici*

Diana Steinhauer[1¤a], **Marie Salat**[1¤b], **Regula Frey**[1], **Andreas Mosbach**[1], **Torsten Luksch**[1], **Dirk Balmer**[1], **Rasmus Hansen**[2¤c], **Stephanie Widdison**[2], **Grace Logan**[2], **Robert A. Dietrich**[3], **Gert H. J. Kema**[4], **Stephane Bieri**[1], **Helge Sierotzki**[1], **Stefano F. F. Torriani**[1], **Gabriel Scalliet**[1]*

1 Syngenta Crop Protection AG, Stein, Switzerland, **2** Syngenta Jealott's Hill Int. Research Centre, Bracknell Berkshire, United Kingdom, **3** Syngenta Biotechnology Inc., Research Triangle Park, North Carolina, United States of America, **4** Wageningen University and Research, The Netherlands

¤a current address: Kelly Scientific Resources, Basel, Switzerland
¤b current address: Novartis Pharma AG, Basel, Switzerland
¤c current address: Wellspring Biosciences, San Diego, California, United States of America
* gabriel.scalliet@syngenta.com

Abstract

Succinate dehydrogenase inhibitor (SDHI) fungicides are widely used for the control of a broad range of fungal diseases. This has been the most rapidly expanding fungicide group in terms of new molecules discovered and introduced for agricultural use over the past fifteen years. A particular pattern of differential sensitivity (resistance) to the stretched heterocycle amide SDHIs (SHA-SDHIs), a subclass of chemically-related SDHIs, was observed in naïve *Zymoseptoria tritici* populations not previously exposed to these chemicals. Subclass-specific resistance was confirmed at the enzyme level but did not correlate with the genotypes of the succinate dehydrogenase (SDH) encoding genes. Mapping and characterization of the molecular mechanisms responsible for standing SHA-SDHI resistance in natural field isolates identified a gene paralog of *SDHC*, termed *ZtSDHC3*, which encodes for an alternative C subunit of succinate dehydrogenase, named alt-SDHC. Using reverse genetics, we showed that alt-SDHC associates with the three other SDH subunits, leading to a fully functional enzyme and that a unique Qp-site residue within the alt-SDHC protein confers SHA-SDHI resistance. Enzymatic assays, computational modelling and docking simulations for the two SQR enzymes (altC-SQR, WT_SQR) enabled us to describe enzyme-inhibitor interactions at an atomistic level and to propose rational explanations for differential potency and resistance across SHA-SDHIs. European *Z. tritici* populations displayed a presence (20–30%) / absence polymorphism of *ZtSDHC3*, as well as differences in *ZtSDHC3* expression levels and splicing efficiency. These polymorphisms have a strong impact on SHA-SDHI resistance phenotypes. Characterization of the *ZtSDHC3* promoter in European *Z. tritici* populations suggests that transposon insertions are associated with the strongest resistance phenotypes. These results establish that a dispensable paralogous gene determines SHA-SDHIs fungicide resistance in natural populations of *Z. tritici*. This study paves

the way to an increased awareness of the role of fungicidal target paralogs in resistance to fungicides and demonstrates the paramount importance of population genomics in fungicide discovery.

Author summary

Zymoseptoria tritici is the causal agent of Septoria tritici leaf blotch (STB) of wheat, the most devastating disease for cereal production in Europe. Multiple succinate dehydrogenase inhibitor (SDHI) fungicides have been developed and introduced for the control of STB. We report the discovery and detailed characterization of a paralog of the C subunit of the SDH enzyme conferring standing resistance towards the SHA-SDHIs, a particular chemical subclass of the SDHIs. The *SDHC* paralog is characterized by its presence/ absence, expression and alternative splicing polymorphisms, which in turn influence resistance levels. The identified mechanisms exemplify the importance of population genomics for the discovery and rational design of the most adapted solutions.

Introduction

Fungicide research is driven by the discovery of molecules with novel modes of action or acting on known targets but either displaying a novel spectrum of biological activity or escaping previously developed resistance mechanisms [1]. During this research process, a very high diversity of molecules is generated to reach the necessary potency and biological spectrum. For single-site fungicides, rational active ingredient (AI) design and empirical chemical scouting are needed to best cover the chemical space of potential inhibitors. A broad biological spectrum is important for disease control. However, this is particularly difficult to achieve for single-site fungicides, mostly because the molecular targets usually show a significant level of variation across pathogens. In addition, the assessment of field populations' sensitivity baselines and the elucidation of cross-resistance patterns are important since they may reveal unexpected variations which then need to be taken into consideration for AI design. SDHIs block the tricarboxylic acid (TCA) cycle through inhibition of the succinate dehydrogenase enzyme (syn. Succinate-ubiquinone oxidoreductase (SQR), EC 1.3.5.1), which is better known as Complex II of the respiratory chain. SDHIs bind to the SQR enzyme at the ubiquinone binding site (Qp-site) which is created by the interface of three of the four enzyme subunits [2, 3]. The fungal SQR is highly variable across species, mainly because of a low sequence conservation of the internal mitochondrial membrane (IMM) SDHC and D subunits [4]. These target variations have a big impact on the biological spectrum of activity of carboxamide SDHIs [5]. Indeed, carboxin, the first molecule of this class introduced in 1966, displayed a basidiomycete spectrum of activity and was mostly used as seed treatment [6, 7]. Major chemistry breakthroughs were needed to expand this biological spectrum to ascomycetes. In 2003, boscalid was released as the first foliar SDHI with a broadened spectrum of activity, enabling the control of diseases caused by ascomycetes [8]. This discovery was shortly followed by the introduction of many other SDHIs covering almost the entire spectrum of fungal diseases. SDHI has been the fastest expanding class of fungicides in the past 15 years with 23 molecules currently listed by the fungicide resistance committee [9, 10]. In particular, some of these novel molecules effectively control the ascomycete *Zymoseptoria tritici*, responsible for the main foliar disease of wheat. *Z. tritici* is the causal agent of Septoria tritici leaf blotch (STB), a major threat to bread and

durum wheat production worldwide and a major driver for fungicide research [11]. Resistance towards SDHIs was readily generated in the lab and caused by non-synonymous mutations within the Qp-site composing subunits encoded by *SDHB*, *SDHC* and *SDHD* [12–14]. Highly differential cross-resistance (XR) profiles were observed for some mutations. In particular, the SDHB_H267Y boscalid-resistant mutants showed increased sensitivity towards fluopyram in *Z. tritici* and multiple other species [13–16]. The field situation is monitored by the industry and academic or governmental research institutes [17–19]. To date, a panel of approximately 20 Qp-site subunit mutation types altering the activity of commercial SDHIs *in vivo* has been reported for *Z. tritici* populations in Europe [19, 20]. The expected impact on field performance is variable depending on the particular mutation-SDHI compound combination [17]. Overall for *Z. tritici*, the SDHI target resistance situation is at a stage of slight expansion in both diversity and frequency of mutations. The speed of resistance development and its practical impact on STB control has been contained, based on recommendations limiting the number of applications in spray programs and the use of mixtures with molecules carrying different modes of action.

To identify novel highly potent SDHI fungicides, we have been exploring a novel subclass of molecules which we termed stretched heterocycle amide SDHIs (SHA-SDHIs) and defined by an aliphatic CC linker instead of an aromatic ring at the amine part of the carboxamide (S1 Fig). Standing resistance towards two SHA-SDHIs, fluopyram and isofetamid has been recently reported in *Z. tritici* European populations [21]. The most tolerant isolates were shown to display practical resistance to the compounds *in planta* but sensitivity to bixafen, another SDHI, was not affected. Since no variation was observed in the sequences of the genes encoding the SQR Qp-site subunits, authors concluded that the mechanism was non-target based [21]. During our research focusing on SHA-SDHIs sensitivity baselines of a large collection of *Z. tritici* field isolates not previously exposed to these molecules were monitored and identified similar resistance to fluopyram. This resistance was specific for the new chemical subclass and not associated with known mutations in SQR genes which was unexpected, since similarly to other fungicides used for STB control such as the QoIs [22–24] or the DMIs [25–27], previously known SDHI resistances emerged through non-synonymous mutations within the target [17, 18]. However, non-target related mechanisms have been reported that may contribute to sensitivity shifts, including increased fungicide efflux caused by the overexpression of the drug transporters *MgMFS1* [28–31] and *ABCt-2* [32], and reduced fungicide uptake caused by an elevation in accumulation of melanin in the fungal cell walls [33].

The primary aim of this study was to characterize the molecular mechanism(s) responsible for SHA-SDHI resistance in *Z.tritici*. We report the mapping and genetic validation of the resistance mechanism, a dispensable paralog of *SDHC* (*ZtSDHC3*) which is present in 20–30% of the European *Z. tritici* population. Differential levels of expression, alternative splicing of *ZtSDHC3* mRNA and a competition between the two SDHC proteins for inclusion into the SQR complex are the main factors modulating resistance. Molecular characterization of promoter sequences for a set of individuals revealed insertions of transposable elements in highly resistant isolates. This level of understanding enabled the careful design and early *in planta* assessment of pydiflumetofen, a novel SHA-SDHI affected by the mechanism but for which the variation has no practical impact on efficacy under normal use conditions. To our knowledge this is the first time that a fungicide target paralog with such complex presence/absence, splicing efficiency and expression polymorphisms has been described in naïve populations and taken into consideration during fungicide optimization.

Results

Z. tritici populations display differential sensitivity to the SHA-SDHI fluopyram

Sensitivity towards commercial fungicides was determined for a set of 99 SHA-SDHI-naïve *Z. tritici* field isolates sampled in Europe between 2006 and 2009. The EC_{50} of these isolates was determined in liquid growth assays and the data obtained compared for each possible pair of SDHI fungicides (cross-resistance (XR) plots, Fig 1). As expected for fungicides with the same mechanism of action, a significant correlation was observed for all SDHIs tested (Pearson, P values < 0.0001) (Fig 1A–1F). However, correlation factors were lower for all fluopyram-paired comparisons (Fig 1A–1C), with *r* values ranging between 0.53 (boscalid vs fluopyram) and 0.56 (benzovindiflupyr vs fluopyram), compared to all the other SDHIs-paired comparisons which were displaying *r* values over 0.74 (Fig 1D–1F). In particular, the three isolates displaying the highest tolerance towards fluopyram (06STD024, 07STGB009 and 09STF011) were highly deviating from the linear correlation and displayed either normal or high sensitivity towards the other SDHIs benzovindiflupyr, boscalid and fluxapyroxad (Fig 1A–1C and 1D–1F). The effect was specifically observed for fluopyram and other research SHA-SDHIs carrying an aliphatic CC linker instead of an aromatic ring at the amine part of the molecule (S1 Fig). Comparative succinate-quinone reductase (SQR) enzyme inhibition tests were performed with mitochondria extracted from a panel of SHA-SDHIs tolerant and sensitive isolates.
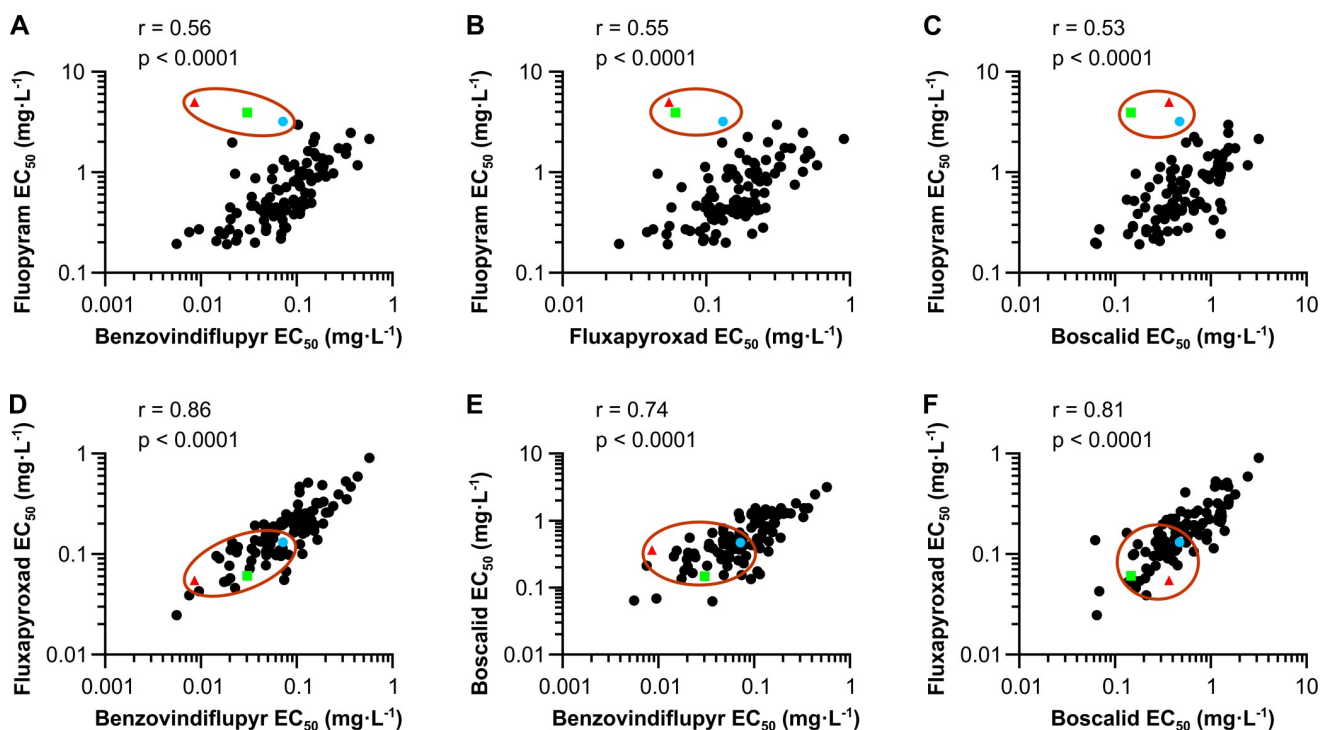
Fig 1. Baseline cross-resistance of Z. tritici populations to SDHI fungicides. Sensitivity towards different SDHIs was determined in liquid culture assays for a collection of 97 Z. tritici strains sampled for fungicide resistance monitoring in 2009 in Europe (plain circles). Two strains 06STD024 (red triangle) and 07STGB009 (green square), were considered fluopyram-resistant in monitoring performed in 2006 and 2007 respectively. 09STF011 (blue circle), belongs to the collection of 97 isolates sampled in 2009 and is the isolate with lowest sensitivity towards fluopyram in this set. Panels (A), (B) and (C) represent liquid culture cross-resistance plots with SHA-SDHI fluopyram on the y axis and non-SHA SDHIs benzovindiflupyr, fluxapyroxad or boscalid on the x-axis respectively. Panels (D), (E) and (F) correspond to cross resistance plots of non-SHA SDHIs fluxapyroxad, benzovindiflupyr and boscalid, compared as pairs. 06STD024, 07STGB009 and 09STF011 are circled in red.

https://doi.org/10.1371/journal.ppat.1007780.g001

Higher IC$_{50s}$ were specifically observed for the SHA-SDHI subclass in mitochondrial extracts from the tolerant isolates indicating a target-based resistance mechanism. However, in SHA-SDHIs/fluopyram tolerant isolates, the target-related resistance mechanism could not be explained by the genotypes of the known *SDHB*, *SDHC* and *SDHD* genes suggesting that other genes were involved in this fluopyram-specific resistance (S1 Dataset).

Mapping of a genetic factor responsible for fluopyram resistance in 06STD024 and 07STGB009 *Z. tritici* isolates

Crosses between *Z. tritici* isolates sensitive (S: IPO323, IPO94269) and resistant (R: 06STD024, 07STGB009) to fluopyram were generated. Mapping populations of 234 and 95 progeny were obtained for crosses IPO323 x 06STD024 and IPO94269 x 07STGB009 respectively. Progeny isolates from both crosses were characterized for their growth (R) / non growth (S) phenotypes on agar plates supplemented with 10 mg.L^{-1} fluopyram (Fig 2A). In both crosses, inheritance of the R phenotype was monogenic (49.5% and 51.5% resistant progeny respectively). A pooled sequencing bulked segregant analysis (BSA) approach was used to map the R locus using pools of genomic DNA from 30 S and 30 R progeny from cross IPO323 x 06STD024. Bulked segregant analysis (BSA) identified a locus on chromosome 3 between positions 3,081,782 and position 3,423,761 of IPO323 genome sequence (342 kb) explaining the difference between the pools with 95% confidence (Fig 2B and S2 Dataset). Fine mapping with the full set of 234 IPO323 x 06STD024 progeny was performed with molecular markers such as cleaved amplified polymorphic sequences (CAPS) and direct PCR length polymorphisms developed from this region (S1 Table). This fine mapping located the resistance factor in an interval of 16 kb from positions 3,200,730 to 3,217,341 of chromosome 3 of IPO323 (Fig 2B).

Within this genomic region, nine genes are predicted in IPO323 (Fig 2B). Only one gene, Mycgr3G70478 encoding a putative P-Type ATPase cation transporter, was predicted to be targeted to the mitochondria (S2 Table). Based on predicted function and subcellular localization, none of these genes could explain in simple terms the specific SHA-shifted SDHI sensitivity profile observed in the SQR enzymatic assay. Sliding-window PCRs were performed on 06STD024 genomic DNA to see whether structural variation may occur at the R locus that would potentially reveal additional genes in the resistant parental strain. This approach resulted in the detection of two large insertions at the mapped locus in the genome of the 06STD024 resistant strain that are not present in IPO323. The first large insertion was 15 kb in size and located at position 3: 3,209,932 of IPO323 genome. The second, over 10 kb in size, was located at position 3: 3,215,008 of IPO323 genome (Fig 2C).

The 15 kb insert of 06STD024 was fully sequenced (GenBank: MK067274), and showed similarity to homologous chromosome 3 regions in other publicly available *Z. tritici* genomes (Fig 2D). Seven putative CDS and a long putative transposon were identified within the locus (Fig 2D). One of these CDS displayed protein sequence similarity to SDHC (XM_003850403, 54% identity). The presence of two short introns within this CDS was confirmed by sequencing of 06STD024 cDNA and the corresponding gene was termed *ZtSDHC3*. *ZtSDHC3*-specific primers amplified this gene only in R parents 06STD024 and 07STGB009, while *SDHC*-specific primers amplified the gene in all (R and S) parental strains. These PCR markers were used to genotype all progeny from crosses IPO323 x 06STD024 and IPO94269 x 07STGB009. For both crosses the presence of *ZtSDHC3* fully segregated with the R phenotype (S1 and S3 Tables). Progeny from cross 07STGB009 x IPO94269 were genotyped with additional CAPS markers from this chromosome 3 locus and confirmed the presence of the *ZtSDHC3* gene at a similar chromosomal location in strain 07STGB009 compared to 06STD024 (S3 Table).
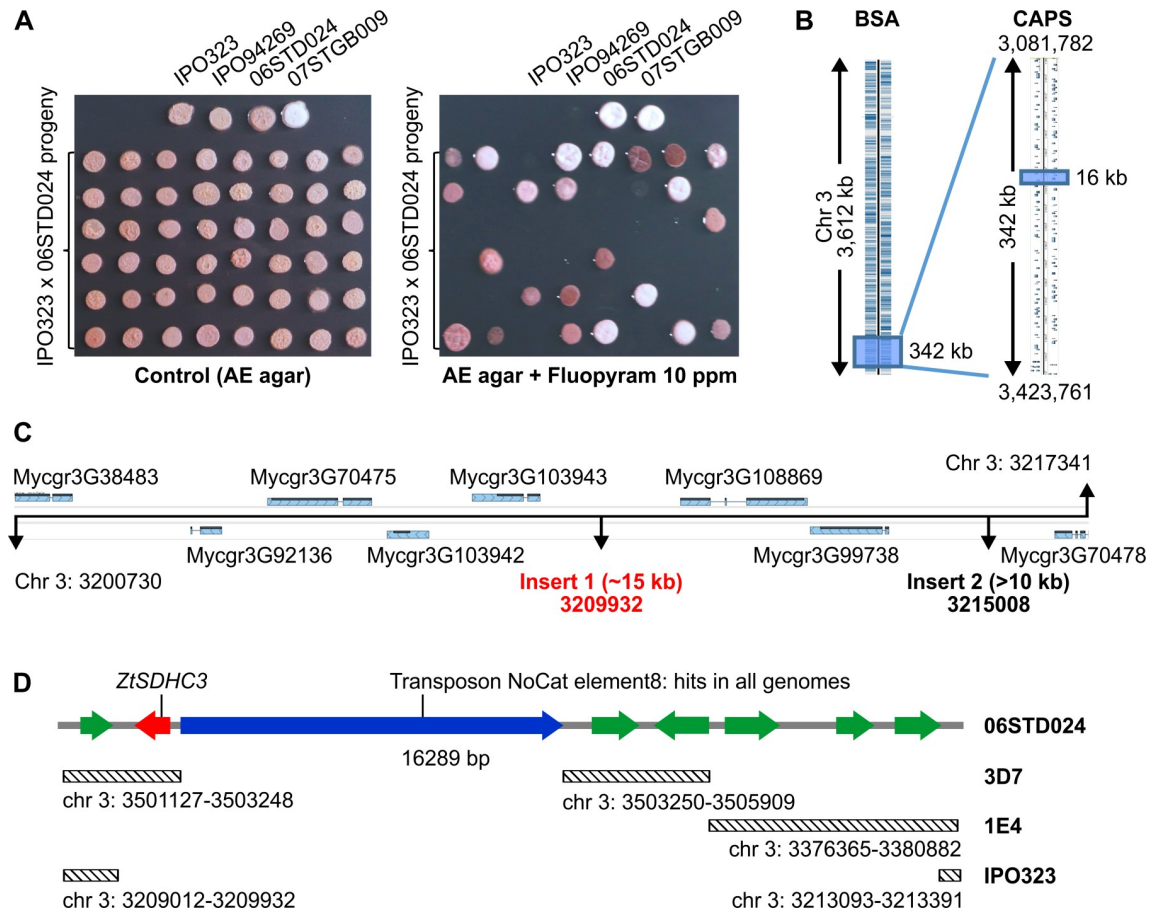
Fig 2. Fine mapping of fluopyram resistance factor using 06STD024 x IPO323 progeny. (A) Agar plate growth assay used for characterizing progeny isolates for resistance or sensitivity to fluopyram. 2 μl of 2.10^6 cells.ml^{-1} were spotted onto AE agar supplemented or not with 10 mg.L^{-1} fluopyram and incubated at 20˚C. Pictures were taken either 7 days (control) or 14 days (fluopyram) after inoculation. (B) IPO323 mapping intervals determined by BSA using 60 progeny isolates (i) and by CAPS markers (ii) on the full mapping population (234 progeny isolates). (C) 16 kb mapping interval of IPO323 chromosome 3. Structural variations at this locus between IPO323 and 06STD024 were determined using long range PCRs. Insert 1 was fully sequenced, only borders of insert 2 were sequenced. Insert 1 and insert 2 positions are based on the IPO323 genome. (D) Gene content of insert 1 region. Predicted genes and their orientation are visualized with arrows, green: putative genes, red: *ZtSDHC3*, blue: transposable element. Diagonally striped rectangles represent regions of high similarity (>90% identity) to other fully assembled *Z. tritici* genomes, corresponding chromosomal coordinates are indicated.

ZtSDHC3 encodes an alternative SDHC subunit responsible for fluopyram / SHA-SDHIs specific resistance

ZtSDHC3 DNA sequence displayed 62% identity to IPO323 *SDHC* (*ZtSDHC1*) CDS. The encoded protein was termed alt-SDHC, its sequence displayed an identity of 54% to IPO323 SDHC. The two nuclear encoded pre-proteins strongly differ at their N-termini. TargetP1.1 [34] predicted N-terminal mitochondrial transit peptides of 36 and 42 amino acids for alt-SDHC and SDHC respectively, that only share 16% identity. The predicted processed protein sequences (SQR cytochrome B subunit without transit peptide) of alt-SDHC and SDHC displayed a much higher similarity (62.5% identity). An alignment of the SDHC paralogs from *Z. tritici* is presented in Fig 3.

Genes encoding for SDHC proteins were identified across a collection of fungal species with available genomes on the Ensembl server (see material and methods). Phylogenetic

Fig 3. *Z. tritici* SDHC proteins alignment. *Z. tritici* ZtSDHC3 (alt-SDHC, NCBI MK067274, isolate 06STD024), ZtSDHC1 (SDHC, Uniprot F9XH52, isolate IPO323) and ZtSDHC2 (SDHC2, NCBI SMR59342, isolate IPO323) proteins were aligned with AlignX (Blosum62). Asterisk (*) is located above the predicted cleavage sites of the pre-proteins indicated by a red line. Red arrow highlights the Qp-site amino-acid residue likely involved in differential SDHI sensitivity pattern.

analysis suggested the presence of 0–2 *SDHC* paralogs in multiple species (S2 Fig). *SDHC* paralogs were identified in multiple clades, but the number of paralogs within a genus appeared species-specific (S4 Table). Another paralog of *ZtSDHC1* was identified in the IPO323 genome (Mycgr3G74581) and named *ZtSDHC2*. The Mycgr3G74581 gene model was modified using the revised gene model of Grandaubert *et al.* [35]. This modified gene model was also found as a correctly predicted gene in the genome of isolate 1E4 (SMR59342). *ZtSDHC2* was present in all the genomes of sequenced *Z. tritici* isolates. Orthologs of *ZtSDHC2* were identified in *Z. brevis*, *Ramularia collo-cygni* and *Mycosphaerella emusae* genomes (S2 Fig). Orthologs of *ZtSDHC2* were not detected in the genomes of the closely related species *Pseudocercospora fijiensis*, *Dothistroma septosporum* and *Baudoinia panamericana*, which all carried an orthologue of *ZtSDHC1*. This phylogenetic analysis suggested that *SDHC* was duplicated in a common ancestor of *Zymoseptoria spp.*, *Ramularia collo-cygni* and *Mycosphaerella emusae* to give *ZtSDHC2*. Species-specific losses of *ZtSDHC2* must have occurred during the evolution of these species. Since *ZtSDHC3* is only found in *Z. tritici* this paralog may be the product of a species-specific duplication event of the *ZtSDHC1* gene. The functional role of *ZtSDHC2* as a possible SQR C-subunit has not been validated. In the *Z. tritici* IPO323 isolate, there is no clear evidence of the expression of this gene in any tested condition (S3 Fig, [36]). Therefore, we concluded that *ZtSDHC1* is the only gene encoding a functional SDHC subunit in isolate IPO323, while isolate 06STD024 likely carries two functional SDHC subunits, SDHC encoded by *ZtSDHC1* and alt-SDHC encoded by *ZtSDHC3*.

To validate that *ZtSDHC3* is responsible for fluopyram / SHA-SDHIs resistance, targeted deletions of *ZtSDHC3* or *ZtSDHC1* were performed in the resistant isolate 06STD024. Targeted gene deletion vectors were constructed using a hygromycin resistance cassette flanked by 1–2 kb of the upstream and downstream genomic sequences of either *ZtSDHC1* or *ZtSDHC3* (see materials and methods). The *ZtSDHC3* deletion mutants of 06STD024 were sensitive to fluopyram and other SHA-SDHIs. Their sensitivity levels were similar to IPO323, a SDHI-sensitive reference isolate (Fig 4A and 4B). The deletion of *ZtSDHC1* in 06STD024 was also achieved. These *SDHC* deletion mutants were more resistant (2 to 10 fold) to SHA-SDHIs than isolate 06STD024 (Fig 4B and S5 Table). The deletion of *ZtSDHC1* was not successful in IPO323, suggesting that *ZtSDHC2*, the unique *SDHC* paralog in this isolate, was not sufficient for maintaining SQR function in this background. IPO323 transformants carrying an ectopic insertion of a vector containing *ZtSDHC3* under the control of a tetracyclin-repressible promoter were obtained (pTet::*SDHC3*, Fig 4A). These IPO323 pTet::*SDHC3*
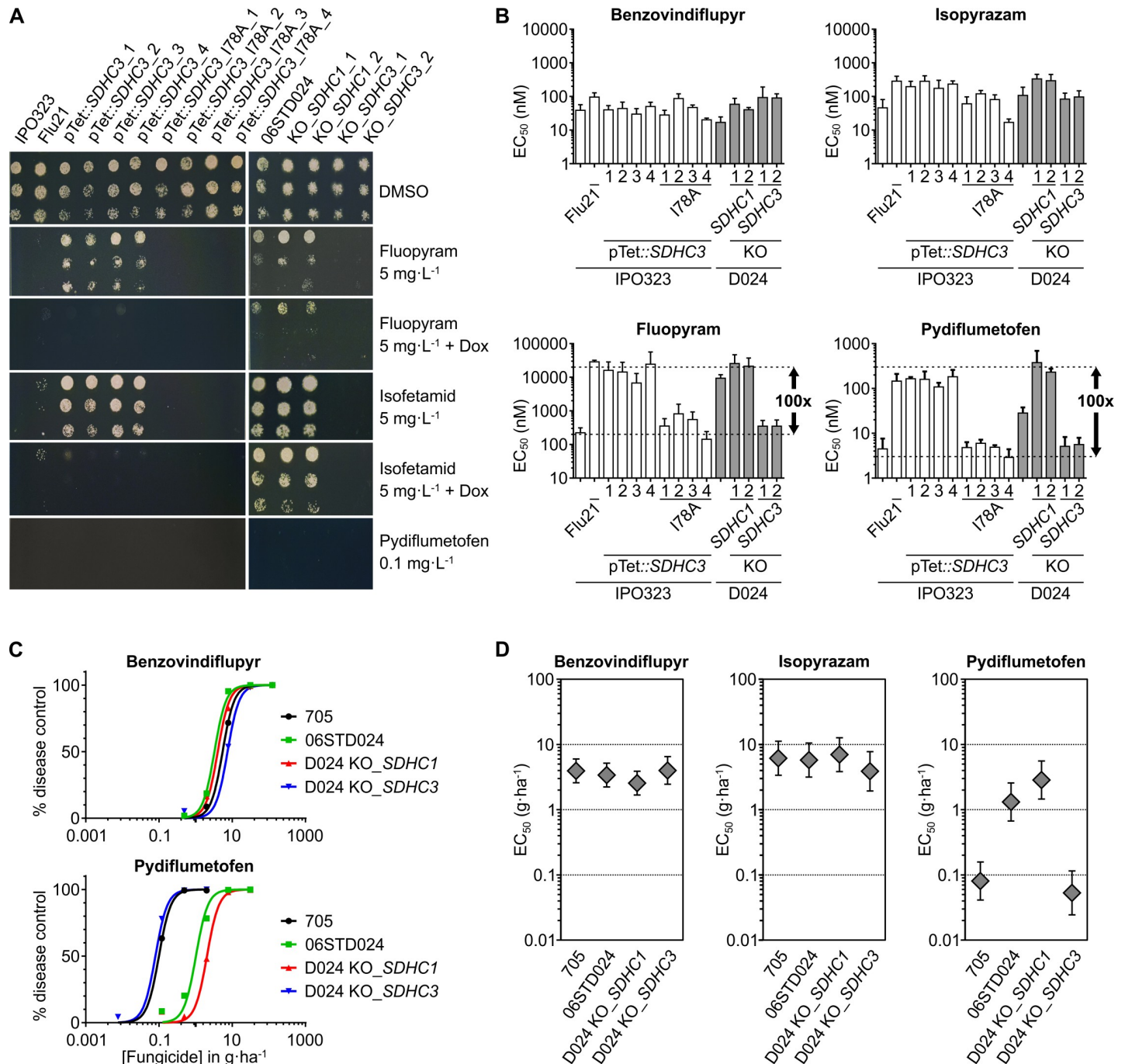
Fig 4. The role of alt-SDHC_I78 residue in conferring SHA-SDHIs-specific resistance *in vivo* and *in planta*. (A) Agar growth phenotypes of IPO323 mutants (left panel) and 06STD024 mutants (right panel). Left panel: Flu21 is an IPO323 SDHC_A84I UV mutant, pTet::*SDHC3*: IPO323 transformants carrying the *ZtSDHC3* gene under the control of a tetracycline-repressible promoter, pTet::*SDHC3*_I78A IPO323 transformants carry a similar construct but contain a mutated version of *SDHC3* gene encoding an alt-SDHC_I78A variant. Right panel: 06STD024 and individual deletion mutants of either the core *ZtSDHC1* (KO_*SDHC1*) or of the dispensable *ZtSDHC3* (KO_*SDHC3*). Pictures were taken at 6DPI, + Dox indicates the addition of doxycycline (30 mg.L^{-1}) to the medium. (B) Liquid culture sensitivity of IPO323 and 06STD024 mutants towards SDHIs. The set of characterized IPO323 (white bars) and 06STD024 (grey bars) mutants was similar to panel A. EC$_{50s}$ (nM) were determined in duplicate in at least 3 biological replicates (see S5 Table). Values obtained for a broader range of marketed and research SDHIs are presented in S5 Table. (C) *In planta* SDHI-sensitivity assays. The presented graphs are derived from a single biological experiment, each value / data point represents the mean disease control value of 12 individual plants. The sensitivity curves were obtained by non-linear regression of the data using GraphPad Prism software. (D) *In planta* EC$_{50s}$ (g.ha^{-1}) of reference strain (705) and 06STD024 mutants for commercial SDHIs, benzovindiflupyr, isopyrazam (non SHA-SDHIs) and pydiflumetofen (SHA-SDHI). Values are derived from four biological replicates of 12 technical replicates each (EC$_{50}$ +/- 95% confidence interval).

https://doi.org/10.1371/journal.ppat.1007780.g004

transformants displayed a SHA-SDHI resistance level similar or slightly superior to the 06STD024 isolate (Fig 4B and S5 Table). The addition of 30 ppm doxycycline did not alter growth on non-selective media, but abolished growth in the presence of the SHA-SDHIs fluopyram and isofetamid (Fig 4A).

Amongst non-conserved positions in the protein alignment shown in Fig 3, isoleucine I78 of alt-SDHC corresponds to an alanine A84 in SDHC. A84 is located within the Qp-site, and is involved in ubiquinone substrate or inhibitor binding [14]. Interestingly, the SDHC_A84I/V substitutions in *Z. tritici* were shown to confer resistance to fluopyram while displaying no effect on sensitivity/resistance to other SDHIs [14, 37]. Therefore, the presence of an isoleucine at position 78 of alt-SDHC could explain the SHA-SDHIs-specific resistance profile conferred by the presence of *ZtSDHC3*.

The involvement of the I78 Qp-site residue of alt-SDHC was tested by expressing an alt-SDHC_I78A variant in IPO323. IPO323 alt-SDHC_I78A transformants displayed similar sensitivity towards SHA-SDHIs as IPO323 or the 06STD024 *ZtSDHC3* knock-out (KO) mutant (Fig 4A and 4B). Overall, these results demonstrated that *ZtSDHC3* is responsible for the fluopyram/SHA-SDHIs-specific resistance profile of 06STD024 and that this gene can functionally replace *ZtSDHC1* in this background. *ZtSDHC3* therefore encodes a dispensable functional C subunit of the *Z.tritici* SQR enzyme whose expression results in SHA-SDHIs specific resistance due to its natural I78 Qp-site residue.

The influence of the *ZtSDHC3*-driven SHA-SDHI resistance for the control of *Z. tritici* during wheat infection was assessed with a small range of commercial SDHIs (Fig 4C and 4D). *In planta* SDHIs sensitivity assays were performed with the 06STD024 isolate and its *ZtSDHC1* or *ZtSDHC3* KO mutants. A control strain (705) devoid of the *ZtSDHC3* gene but more aggressive than IPO323 on wheat variety Riband was also included for comparison (Fig 4C and 4D).

On untreated plants, 06STD024 *ZtSDHC3* and *ZtSDHC1* KOs displayed infection levels similar to wild type. *In planta* sensitivities towards the non SHA-SDHIs benzovindiflupyr and isopyrazam were similar across the isolates (Fig 4D). Conversely, the presence of *ZtSDHC3* impacted sensitivity towards the SHA-SDHI compound pydiflumetofen *in planta* (Fig 4C and 4D). Similarly to liquid culture assays, the most tolerant isolate was 06STD024 *ZtSDHC1* KO which displayed an *in planta* EC_{50} 53 fold higher than 06STD024 *ZtSDHC3* KO mutant (2.85 g.ha^{-1} and 0.053 g.ha^{-1} respectively) (Fig 4D). By contrast, the WT isolate 06STD024 displayed a reduced *in planta* EC_{50} of 1.31 g.ha^{-1} which corresponds to a sensitivity difference of 25 fold compared to the *ZtSDHC3* KO mutant (Fig 4D).

Our data validate the effect of *ZtSDHC3* on *Z.tritici* sensitivity towards commercial SHA-SDHIs *in planta*. The activity of pydiflumetofen on the most SHA-SDHI-shifted *Z. tritici* GM isolate was similar to that of benzovindiflupyr on wild type isolates as the intrinsic potency of pydiflumetofen is higher.

Enzymatic tests reveal distinct sensitivity profiles for SDHC and alt-SDHC SQRs

Succinate-ubiquinone oxidoreductase (SQR) inhibition assays were performed on mitochondrial extracts from a panel of strains that were (i) either carrying a unique C-subunit encoding gene (*ZtSDHC1*, *ZtSDHC1_A84I* or *Zt-SDHC3*), or (ii) carrying two C-subunit encoding genes *ZtSDHC1* and *ZtSDHC3* (Table 1).

As expected, mitochondrial extracts from strains carrying only the *ZtSDHC1* gene (IPO323 and 06STD024 *SDHC3* KO) were displaying similar WT-SQR sensitivity profiles (Table 1). Conversely, mitochondrial extracts from a strain carrying the pure altC-SQR (06STD024

Table 1. Succinate-quinone SDHIs sensitivity assays on purified mitochondria of field isolates and transformants of *Z. tritici*.

Compounds	Succinate-quinone IC_{50} (nM)[a]													
	IPO323	IPO323_Flu21		06STD024		D024 *SDHC3* KO		D024 *SDHC1* KO		pTet Induced		pTet Repressed	
	SDHC	SDHC_A84I	RF[b]	SDHC / altC	RF	SDHC	RF	altC	RF	SDHC / altC	RF	SDHC / altC	RF
Carboxin	969.0 ± 182.1	1152.9 ± 152.7	1.2	730.7 ± 84.4	0.8	775.1 ± 94.5	0.8	865.0 ± 214.9	0.9	762.5 ± 163.7	0.8	1196.5 ± 85.0	1.2
Boscalid	17.0 ± 3.7	62.0 ± 19.2	3.6	61.9 ± 16.0	3.6	16.4 ± 2.4	1.0	54.4 ± 12.9	3.2	40.3 ± 2.7	2.4	29.8 ± 4.0	1.8
Penthiopyrad	1.4 ± 0.3	4.6 ± 1.7	3.3	2.0 ± 0.8	1.4	1.5 ± 0.3	1.1	1.6 ± 0.7	1.2	1.8 ± 0.1	1.3	1.9 ± 0.4	1.4
Bixafen	1.4 ± 0.1	3.2 ± 0.5	2.3	1.8 ± 0.7	1.3	1.3 ± 0.2	1.0	2.1 ± 0.6	1.5	1.8 ± 0.4	1.3	1.5 ± 0.6	1.1
Fluxapyroxad	4.3 ± 1.1	5.1 ± 0.7	1.2	3.5 ± 0.3	0.8	3.3 ± 0.8	0.8	3.1 ± 0.4	0.7	3.3 ± 0.6	0.8	4.5 ± 1.0	1.1
Isopyrazam	0.8 ± 0.1	5.2 ± 2.6	6.4	2.6 ± 0.6	3.3	0.6 ± 0.2	0.7	2.4 ± 0.5	2.9	1.7 ± 0.4	2.1	1.2 ± 0.3	1.5
Benzovindiflupyr	0.7 ± 0.2	1.0 ± 0.2	1.4	0.5 ± 0.17	0.8	0.6 ± 0.11	0.8	0.6 ± 0.05	0.9	0.5 ± 0.09	0.8	0.5 ± 0.03	0.8
Fluopyram	12.5 ± 2.0	1440.9 ± 354.3	115.6	1387.3 ± 522.2	111.3	10.1 ± 2.0	0.8	1164.4 ± 201.2	93.4	547.5 ± 68.8	43.9	21.9 ± 7.7	1.8
Compound 1	113.0 ± 10.9	2566.0 ± 238.6	22.7	874.7 ± 158.9	7.7	79.4 ± 7.6	0.7	940.2 ± 238.3	8.3	484.1 ± 42.8	4.3	152.5 ± 17.5	1.4
Compound 2	5.3 ± 0.6	780.2 ± 156.6	146.5	415.2 ± 68.0	78.0	3.7 ± 0.5	0.7	357.6 ± 63.4	67.1	204.0 ± 20.7	38.3	15.6 ± 3.9	2.9
Compound 3	0.7 ± 0.2	28.0 ± 7.3	41.9	26.4 ± 1.2	39.5	0.8 ± 0.13	1.2	22.7 ± 0.8	34.0	nd[c]	-	nd	-
Pydiflumetofen	0.3 ± 0.04	2.0 ± 0.4	6.2	1.4 ± 0.05	4.6	0.3 ± 0.07	1.1	1.5 ± 0.4	4.9	0.9 ± 0.3	2.8	0.5 ± 0.1	1.7
Isofetamid	0.9 ± 0.1	21443.3 ± 4551.8	22876	nd[c]	-	nd	-	>50000	>55000	nd	-	nd	-

[a] Values are the mean of three independent IC_{50} determinations and expressed in nM ± standard deviation.

[b] Resistance factor (RF) corresponding to IC_{50} ratio compared to IPO323 values.

[c] Not determined (nd).

Field isolates: IPO323 and 06STD024, IPO323_Flu21: UV mutant of IPO323 carrying the SDHC_A84I mutation [14], D024 *SDHC1* KO and D024 *SDHC3* KO: deletion mutants of either the core*ZtSDHC1* (SDHC) or of the alternative-*ZtSDHC3* (alt-SDHC) gene in 06STD024 background, pTet Induced and pTet Repressed: IPO323 pTet::*SDHC3* transformant grown in the absence (induced) or presence (repressed) of 30 mg.L^{-1} doxycycline.

SDHC1 KO) displayed higher IC_{50} values towards the full panel of SHA-SDHIs tested. The resistance factors ranged between 4.9 for pydiflumetofen to over 55'000 for isofetamid. The resistance factors displayed by the altC-SQR enzyme were very similar to the ones displayed by the C_A84I-SQR mutant, confirming the main involvement of alanine to isoleucine substitution in driving the SHA-SDHIs subclass-specific resistance.

Interestingly, resistance factors displayed by SQR extracted from 06STD024 were very similar to the ones displayed by 06STD024 *SDHC1* KO, suggesting that WT-SQR was absent or highly depleted in the mitochondrial extracts of this isolate. The resistance factors displayed by altC-SQR (06STD024 *SDHC1* KO) were about two fold higher than the ones obtained for an IPO323 pTet::*SDHC3* ectopic transformant grown under inducible conditions (pTet Induced, Table 1). These lower IC_{50s} suggest that a relevant proportion of WT-SQR was still present in the mitochondria of the IPO323 transformant, limiting the observed shift. Finally, the same IPO323 pTet::*SDHC3* ectopic transformant grown under repressive condition (30 ppm doxycycline) was displaying SQR sensitivity profiles similar to WT-SQR, suggesting a very low abundance of the altC-SQR in the mitochondria of the transformant.

These results are consistent with a mixture of the two types of SQR enzymes being simultaneously present and functional. They also suggest the presence of mixed SQR populations mitigating the observed sensitivity shift due to differing ratios of the two types of C subunits.

Molecular docking within 3D models of SQR variants explains differential potency and cross resistance among SHA-SDHIs

Very significant potency and sensitivity variations have been observed across the SHA-SDHIs molecules that were tested against *Z. tritici* SQR variants (Table 1). These differences have a major practical impact for the control of the disease. For example, a selection of SHA-SDHIs

tolerant *Z. tritici* isolates were recently shown to display *in planta* resistance towards isofeta-mid and fluopyram at agronomically-relevant use rates [21]. These results are aligned with our enzyme assays in which isofetamid displayed a high potency on WT-SQR (IC_{50} = 0.9nM) but totally failed to inhibit altC–SQR (RF>55'000) and in which fluopyram combined moderate potency (IC_{50} = 12.5nM) on WT-SQR with an approximate 100 fold resistance on the altC-SQR (Table 1). To achieve disease control, molecules combining high potency and lim-ited resistance factors like pydiflumetofen are highly desired. To design such molecules, it is essential to understand the factors driving potency and resistance at an atomistic level. To ten-tatively explain why pydiflumetofen escapes practical resistance caused by *ZtSDHC3* (Fig 4D), 3D homology models for the WT- and altC-SQR were generated and comparative docking studies carried out.

The superposition of WT and alternative SQR models showed that the two enzymes are structurally highly conserved. In particular all Qp site residues are conserved except SDHC_A84 which corresponds to I78 in alt-SDHC (Figs 3 and 5A). In agreement with this, C_A84I- and altC-SQR enzymes displayed highly similar SDHI sensitivity profiles (Table 1). Molecular docking of SHA-SDHIs into the homology models of the *Z.tritici* SQR variants have been carried out and protein-ligand interactions analyzed. The interaction of carboxamide SDHIs with the SDHC_A84 residue and C_A84V/I-SQR mutants has been described previ-ously [14]. It was found that the linker of fluopyram, which is interacting via Van der Waals forces with SDHC_A84 cannot be properly accommodated with an isoleucine at position 84 [14]. These findings and assumptions remain true for fluopyram interaction with the I78 posi-tion of altC-SQR.

Molecular docking of isofetamid into the WT-SQR predicts hydrogen bonds between the amide oxygen of the molecule and SDHD_Y130 and SDHB_W224 residues (Fig 5D). The nitrogen of the amide forms a hydrogen bond to SDHC_S83 mediated by a water molecule. The carbonyl oxygen of isofetamid SHA aliphatic chain is not involved in a hydrogen bond to SQR but plays an important role together with the gem di-methyl group for the pre-organiza-tion of the molecule into the bioactive conformation. In particular, the ortho methyl substitu-ent stabilizes a conformation of the phenyl ring in which Van-der-Waals interactions to SDHC_A84 can be formed. In addition, the para isopropyloxy substituent is at the right dis-tance in the model to form Van-der-Waals interactions to SDHC_V88. Contrastingly, in altC-SQR the isoleucine 78 of alt-SDHC reduces the size of the binding pocket. Docking of iso-fetamid into the smaller binding pocket of altC-SQR did not result in any energetically favor-able conformation. Maintaining an isofetamid conformation similar to the one obtained in WT-SQR leads to a steric clash of the phenyl ring with alt-SDHC_I78 which is in agreement with the very high resistance factors (>20'000 fold) observed in the altC-SQR and C_A84I-SQR mutants (Table 1).

In contrast, pydiflumetofen is highly potent on WT-SQR (EC_{50} = 0.3nM) and is only shifted by a factor of 6 in the isoleucine SQRs (C_A84I and altC-SQR) (IC_{50} = 2.0 nM). To our knowl-edge, this is a unique behavior within SHA-SDHIs. To assign how distinct parts of the chemi-cal structure of pydiflumetofen contribute to the favorable activity and resistance profile, molecules have been selected for analysis that belong to the same chemical series of pydiflume-tofen but differ only by single chemical transformations (matched pairs, compounds 1–3 shown in Fig 5C). The putative binding mode of pydiflumetofen in complex with the classical and alternative SQR are shown in Fig 5B and 5E.

Similarly to other carboxamide SDHIs, the binding interaction of pydiflumetofen with the Qp site involves hydrogen bonds with SDHD_Y130 and SDHB_W224 through the carbonyl oxygen of the amide bound. The specific SHA-SDHI CC linker of pydiflumetofen bears a ste-reo center. The role of this stereo center is elucidated by comparing two related SDH inhibitors
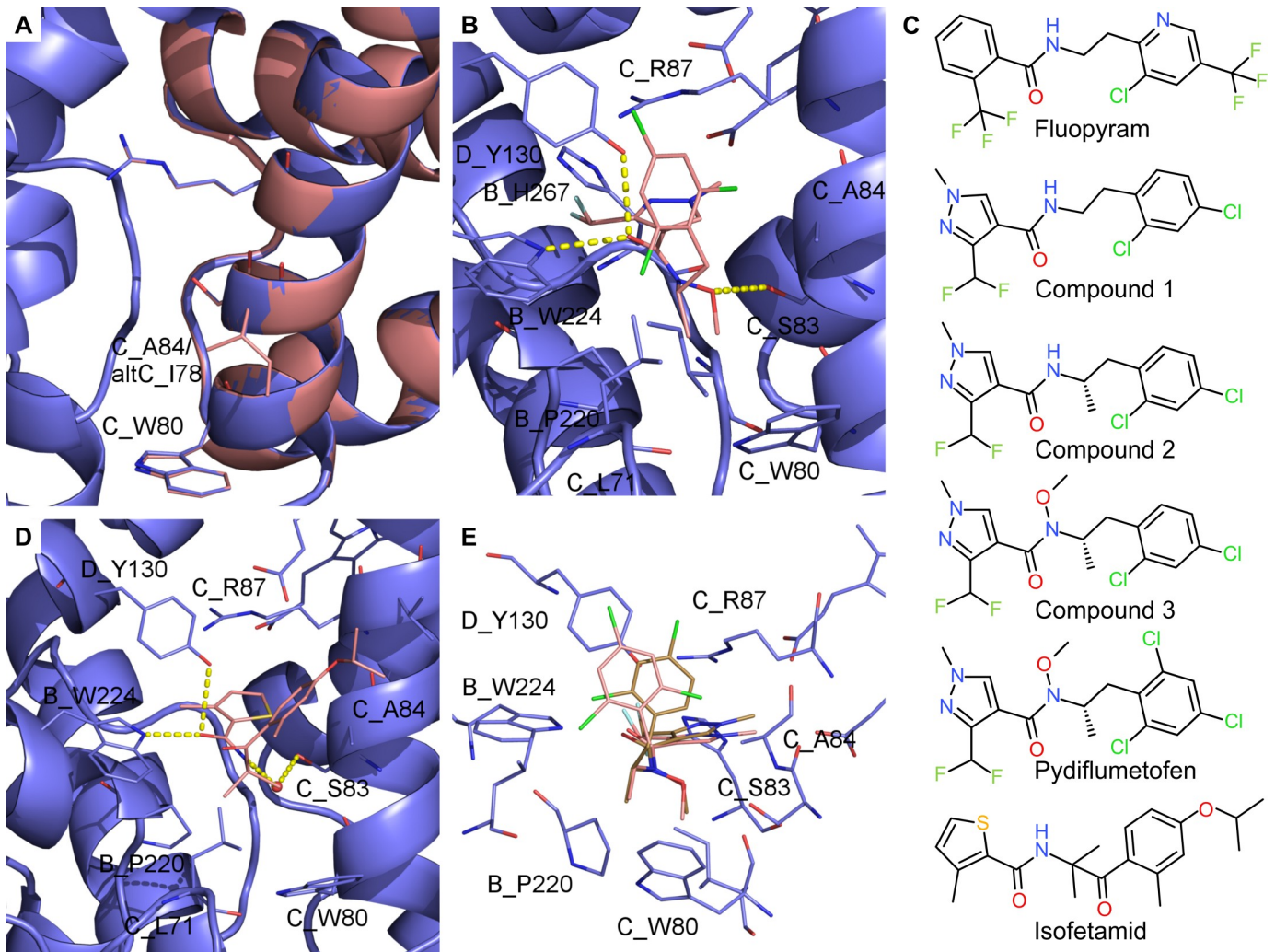
Fig 5. Comparison of *Z. tritici* 3D models of the two SQR paralogs and putative binding modes for SHA SDHIs. (A) Homology model of *Z. tritici* WT-SQR (blue) superimposed on the homology model of *Z. tritici* altC-SQR (salmon). (B) Putative binding mode of pydiflumetofen in *Z. tritici* WT-SQR. (C) 2D depiction of SDH inhibitors used for docking comparisons and discussed in the text. (D) Putative binding mode of isofetamid in *Z. tritici* WT-SQR. E. superposition of energy minimum conformations for pydiflumetofen and compound 3.

for which the only difference is a methyl group: compound 1, a molecule bearing an ethyl linker without methyl group and stereo center, is more flexible and multiple low energy conformations exist. A pre-organization is caused by the additional methyl group in compound 2, which also introduces a stereo center (R and S enantiomers). The S enantiomer is predicted to adopt a low energy conformation more compatible with the shape of the ubiquinone binding pocket. This pre-organized conformation leads to a favorable entropic effect that is predicted to increase the activity. The IC_{50} for compound 2 is indeed lower in comparison to compound 1 on WT-SQR but the magnitude of the effect (21 fold) is more pronounced than predicted. The same trend is observed in isoleucine SQR (SDHC_A84I) but in this case leading to only a 3 fold increased activity for compound 2 compared to compound 1.

A very special feature of pydiflumetofen is its substituted N-methoxy amide. While all other carboxamide SDHIs are predicted to form hydrogen bonds to SDHC_S83 mediated by a water molecule, pydiflumetofen is predicted to form a direct hydrogen bond of the methoxy oxygen

to the serine (Fig 5B). This hypothesis is in line with various crystal structures in which ubiquinone analogues are bound to SQR (e.g. pdb code 5C3J), and form direct hydrogen bonds to the serine. In addition, in the model the methyl moiety of the N-methoxy amide forms lipophilic interactions with isoleucine 269 and proline 220 of SDHB. This might be the reason for the 7.6 fold increased potency of N-methoxy amide-containing compound 3 compared to the matched pair compound 2 (without N-methoxy amide). The resistance factors are reduced to 42 or 39.5 fold for compound 3 in comparison to 146 or 78 fold for compound 2 which is hypothesized to be due to positive lipophilic interactions to I84 or I78 in the SDHC or alt-SDHC SQR variants respectively.

Interestingly the addition of a third chlorine atom in the aromatic ortho position significantly decreases the resistance factor from 42 fold for compound 3 to 6 fold for pydiflumetofen. A conformational analysis showed that the aromatic ring is rotated further away from SDHC_A84 in comparison to compound 3 in the energy minimum conformation of pydiflumetofen (Fig 5E). It is assumed that this particular conformational effect reduces the steric hindrance in altC-SQR.

Polymorphism of *alt-SDHC* in *Z. tritici* field populations: Presence/absence, expression and splicing

The presence/absence polymorphism of *ZtSDHC3* and *ZtSDHC1* in *Z. tritici* field populations was determined using PCR specific for each gene (see materials and methods). The *ZtSDHC3* gene was detected at frequencies ranging from 17% to 31% in the EU depending on the year of sampling whereas the *ZtSDHC1* gene was detected in all isolates (Table 2). 123 *Z. tritici* genomes [38] corresponding to isolates collected in four locations (Switzerland, USA, Israel, Australia) prior to the introduction of SDHIs for disease control in wheat were screened *in silico*. The *ZtSDHC3* gene was found in 29% of Swiss isolates and in 18% of the USA (Oregon) isolates. Interestingly, the gene was not detected in the 25 isolates from Israel but was present in all isolates from Australia.

ZtSDHC3 sequences were determined by Sanger or Illumina amplicon sequencing for a panel of 154 isolates carrying the gene (EU collections from Table 2). We identified 12 nucleotide haplotypes (S6 Table), among which 11 were rare variants of the main canonical sequence and represented only once in the panel (0.6%). Among these variants, six carried non-synonymous mutations affecting the alt-SDHC protein sequence. Three corresponded to truncated likely inactive forms of the protein and three corresponded to likely functional R34Q, S66Y and T73S protein variants. In comparison, for 350 strains (2016 collection) sequenced at the *ZtSDHC1* gene locus, 206 different nucleotide haplotypes were identified for a total of 27 different SDHC protein variants (S3 dataset). This relatively rare occurrence of mutations within

Table 2. Occurrence of the *ZtSDHC3* gene in European *Z. tritici* monitoring populations and the pangenome.

	EU monitoring				Pangenome			
					Switzerland	USA	Israel	Australia
	2009	2010	2011	2016	1999	1990	1992	2001
Present	16	30	19	102	11	9	0	21
Absent	80	66	77	282	27	41	25	0
Total	96	96	96	384	38	50	25	21
Frequency (%)	16.7	31.3	19.8	26.6	28.9	18	0	100

Shaded grey area corresponds to available *Z. tritici* genomes [38].

https://doi.org/10.1371/journal.ppat.1007780.t002

the *ZtSDHC3* gene is highly contrasting with the high degree of polymorphisms observed for the core *ZtSDHC1* gene.

Liquid culture and plate growth SDHI sensitivity assays were performed on a cohort of 93 field isolates collected in 2009 and characterized for the presence/absence of the *ZtSDHC3* gene (Fig 6A and 6B). Liquid culture assay validated a significant difference between the two groups with SHA-SDHI fluopyram (t test, p<0.05) but not with non SHA-SDHI benzovindiflupyr (Fig 6A). However, the panel of *ZtSDHC3* containing isolates displayed a wide range of fluopyram EC_{50} varying from sensitive (0.3 mg.L^{-1}) to resistant (up to 3.2 mg.L^{-1}). The growth/no growth phenotype on SHA-SDHI supplemented agar plates of these 93 field isolates mostly correlated with the presence/absence of the *ZtSDHC3* gene (Fig 6B). However, depending on the SHA-SDHI used for the assay, significant growth/sensitivity differences are visible across- the isolates carrying the *ZtSDHC3* gene. Among SHA-SDHIs, isofetamid was the compound for which the presence of the gene gave the clearest correlation (presence = growth, absence = no growth). Only one isolate carrying the gene, 09STIR20.1 did not grow on isofetamid-supplemented agar plate (10 DPI, 5 mg.L^{-1}), which is in agreement with our observation of a loss of function frameshift mutation in the *ZtSDHC3* gene in this strain (position 78 in Fig 6B and S6 Table). On fluopyram-supplemented plate (18 DPI, 5 mg.L^{-1}), a longer incubation
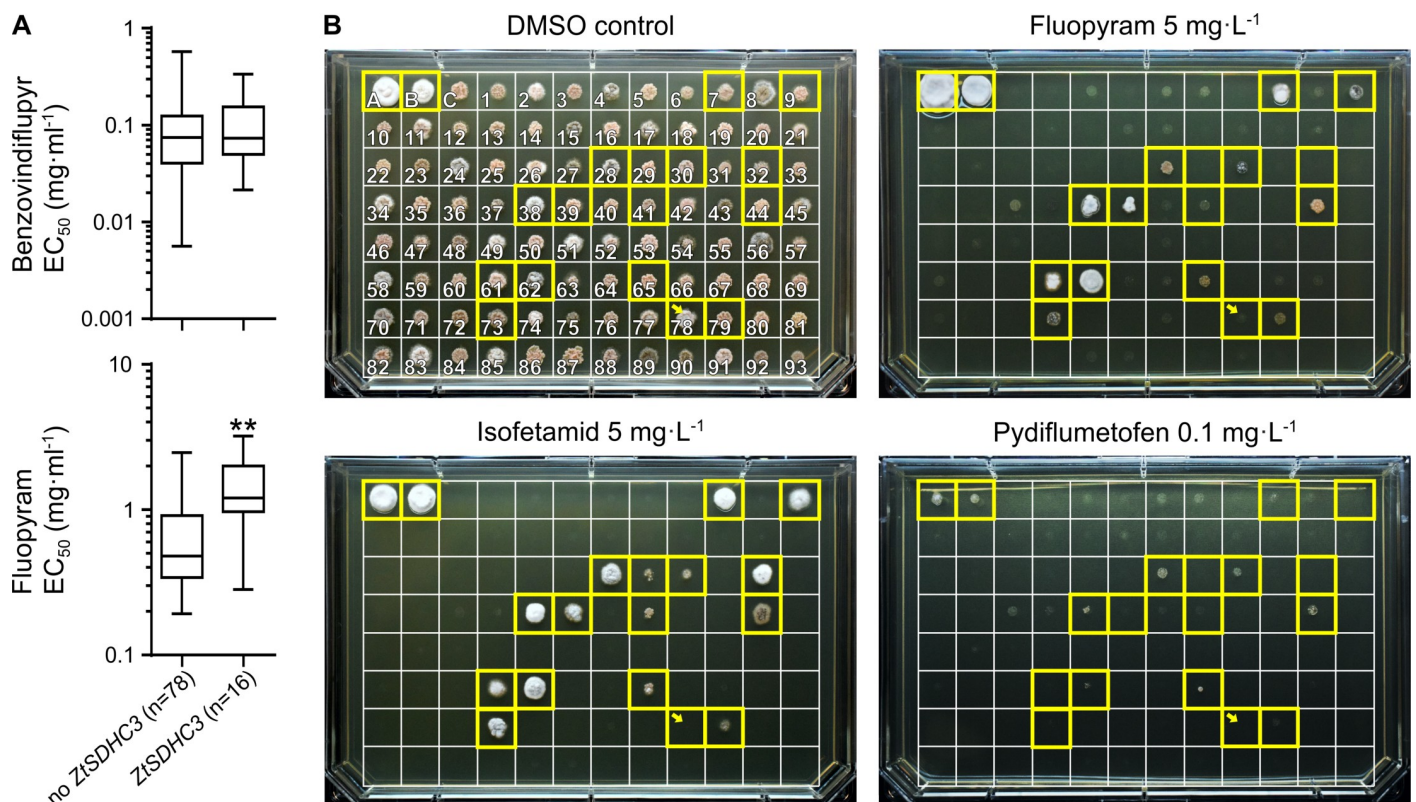
Fig 6. Resistance to SHA-SDHIs in *Z. tritici* EU populations. (A) Box and whisker plot presenting EC_{50} sensitivity data of 93 *Z. tritici* isolates sampled in the EU in 2009. Sensitivity data are sorted by genotype according to the presence of the *ZtSDHC3* gene. ** p value of 0.0029 in Welch's corrected unpaired t-test. (B) Solid agar growth of a collection of 93 *Z. tritici* isolates sampled in 2009 (same set as above). Individual strains from this collection are boxed and numbered 1 to 93. Boxes A and B correspond to reference resistant strains 06STD024 and 07STGB009 respectively. Box C corresponds to IPO323 reference sensitive isolate. The yellow framed boxes correspond to strains carrying the *ZtSDHC3* gene. Yellow arrow designates strain 09STIR20.1 (number 78) carrying a non-functional alt-SDHC (frameshift, S6 Table). Each individual strain was spotted onto AE agar plates (approx. 700 cells per spot) supplemented or not with isofetamid 5 mg.L^{-1}, fluopyram 5 mg.L-1 and pydiflumetofen 0.1 mg.L^{-1}. Plates were left to grow at 20°C in the dark and imaged at 10 DPI (DMSO control and isofetamid) or 18 DPI (fluopyram and pydiflumetofen).

https://doi.org/10.1371/journal.ppat.1007780.g006

was required to distinguish a wide range of growth phenotypes for the *ZtSDHC3* containing strains, these varied from strong growth to no growth at all, including strains encoding a functional alt-SDHC protein. Under these conditions, some background growth started to become visible for isolates devoid of the *ZtSDHC3* gene (positions 4–5 in Fig 6B). However, only *ZtSDHC3* containing strains displayed strong to moderate growth in the assay. Finally, for pydiflumetofen, in addition to an extended incubation, the concentration of the molecule needed to be reduced by 50 fold (18 DPI, 0.1 mg.L^{-1}) to observe weak growth with resistant controls 06STD024 and 07STGB009 and with some but not all of the isolates that displayed a strong growth on fluopyram-supplemented plates (compare positions 28, 44 or 61, 62 in Fig 6B). Also for this compound, background growth started to become visible for a range of isolates not carrying *ZtSDHC3* (positions 4, 5 in Fig 6B). This effect was even more pronounced than with fluopyram, suggesting that other mechanisms besides the presence of *ZtSDHC3* are also relevant for baseline sensitivity differences to this molecule in the population.

These growth assay results are in good agreement with the different potency and resistance factors observed in SQR assays for SHA-SDHIs (Tables 1 and 3). In order to characterize in more depth the mechanisms driving sensitivity differences across the isolates, a subset of eight isolates carrying the *ZtSDHC3* gene was analyzed for their sensitivity to SDHIs, alt-SDHC expression and splicing patterns. Liquid culture growth sensitivity tests were performed to determine EC$_{50s}$ for this set of isolates towards a wide range of commercial and research SDHIs (S5 Table). The resistance factors obtained for fluopyram and pydiflumetofen in liquid

Table 3. Overview of genotyping, phenotyping and protein assays for a panel of *Z. tritici* field isolates.

	Gene	mRNA				Mitochondrial Protein			Fluopyram		Isofetamid		Pydiflumetofen	
Strain	*ZtSDHC3*[a]	*ZtSDHC1*[b]	*ZtSDHC3*[b]	Splice ratio[c]	Gel band[d]	SDHC[e]	alt-SDHC[e]	Total C[e]	RF LC[f]	Growth[g]	RF LC	Growth	RF LC	Growth
IPO323	no	1.6E6 ± 3.1E5	-	-	-	41.9 ± 20.5	-	41.9 ± 20.5	1	No	nd*	No	1	No
IPO94269	no	6.7E5 ± 8.4E4	-	-	-	21.1 ± 3.3	-	21.1 ± 3.3	0.7	No	nd	No	1.1	No
09STIR20.3	yes	3.5E5 ± 7.4E4	3.0E4 ± 6.1E3	Neg	-	39.6 ± 20.9	2.0 ± 1.3	41.6 ± 22.2	1.9	Very weak	nd	Weak	1.8	Very weak
09STD053	yes	4.2E5 ± 8.9E4	4.0E4 ± 7.1E3	6.9	-	27.1 ± 13.0	48.6 ± 17.0	75.7 ± 30.0	2.5	Weak	nd	Strong	1.4	No
09STD041	yes	6.0E5 ± 2.4E5	5.4E4 ± 1.1E4	2.9	-	4.9 ± 4.9	46.3 ± 22.3	51.3 ± 27.2	6.2	Weak	nd	Strong	4.4	Very weak
09STF037	yes	6.2E5 ± 2.0E5	5.7E4 ± 1.2E4	22.7	Very weak	5.1 ± 2.8	55.4 ± 3.2	60.5 ± 6.0	2.1	Very weak	nd	Weak	1.8	Very weak
09STF011	yes	2.7E5 ± 5.8E4	1.6E5 ± 2.2E4	59.5	Weak	7.8 ± 3.5	38.6 ± 5.0	46.4 ± 8.5	16.1	Moderate	nd	Strong	4.0	Weak
09STF112	yes	1.1E6 ± 2.3E5	1.0E5 ± 2.0E4	49.7	Weak	4.6 ± 0.4	57.7 ± 9.7	62.3 ± 10.1	13.0	Strong	nd	Strong	4.2	Very weak
07STGB009	yes	1.5E5 ± 2.2E4	1.6E6 ± 2.1E5	73.3	Strong	0.4 ± 0.7	133.2 ± 15.9	133.7 ± 16.6	49.2	Very strong	nd	Very strong	5.5	Weak
06STD024	yes	9.6E4 ± 2.9E4	3.6E6 ± 3.9E5	86.9	Strong	-	97.2 ± 47.0	97.2 ± 47.0	42.1	Very strong	nd	Very strong	6.3	Weak

[a] *ZtSDHC3* gene presence determined by PCR.

[b] Absolute copy number per µg of total RNA (average values), correspond to "*ZtSDHC1*" and "*ZtSDHC3* total" Fig 7B. Values correspond to the mean of 8 individual determinations ± SD.

[c] *ZtSDHC3* mRNA splicing ratio in percent, inferred from qPCR assays shown in Fig 7B.

[d] Inferred from visual inspection of gel electrophoresis presented in Fig 7A.

[e] LC-MS/MS quantification of the SDHC and alt-SDHC proteins in mitochondrial extracts (fmol). Values presented correspond to the mean of 6 individual determinations on the same set of samples ± SD.

[f] Resistance factor (RF) in liquid culture assays (LC) respective to IPO323 (S5 Table).

[g] Growth phenotype on SDHI-amended plate, inferred from assays following procedure described in Fig 6.

* not determined;—not detected.

https://doi.org/10.1371/journal.ppat.1007780.t003

culture assays are in good agreement with growth phenotype on solid agar at fixed concentration (Table 3). These experiments support a wide range of fluopyram SHA-SDHI resistance levels relative to IPO323 (devoid of the *ZtSDHC3* gene), from 2 fold for 09STIR20.3 to almost 50 fold for 06STD024 and 07STGB009 (Tables 3 and S5). We hypothesized that these differences in resistance levels among *ZtSDHC3*-carrying isolates are driven by differences in its expression. Indeed, semi-quantitative RT-PCR and hydrolysis probe RT-qPCRs revealed varying proportions of spliced and unspliced *ZtSDHC3* mRNA across the range of tested isolates (Fig 7A and 7B). Total *ZtSDHC3* mRNA correlated with increased splicing efficiency (Fig 7C and Table 3). This efficiency ranged between not measurable for the most sensitive isolate 09STIR20.3, to 73% and 87% for the most SHA-SDHI resistant isolates 07STGB009 and 06STD024 respectively. Moderately resistant isolates 09STF011 and 09STF112 displayed less of the spliced form, which represented 59% and 50% of total *ZtSDHC3* mRNA respectively.
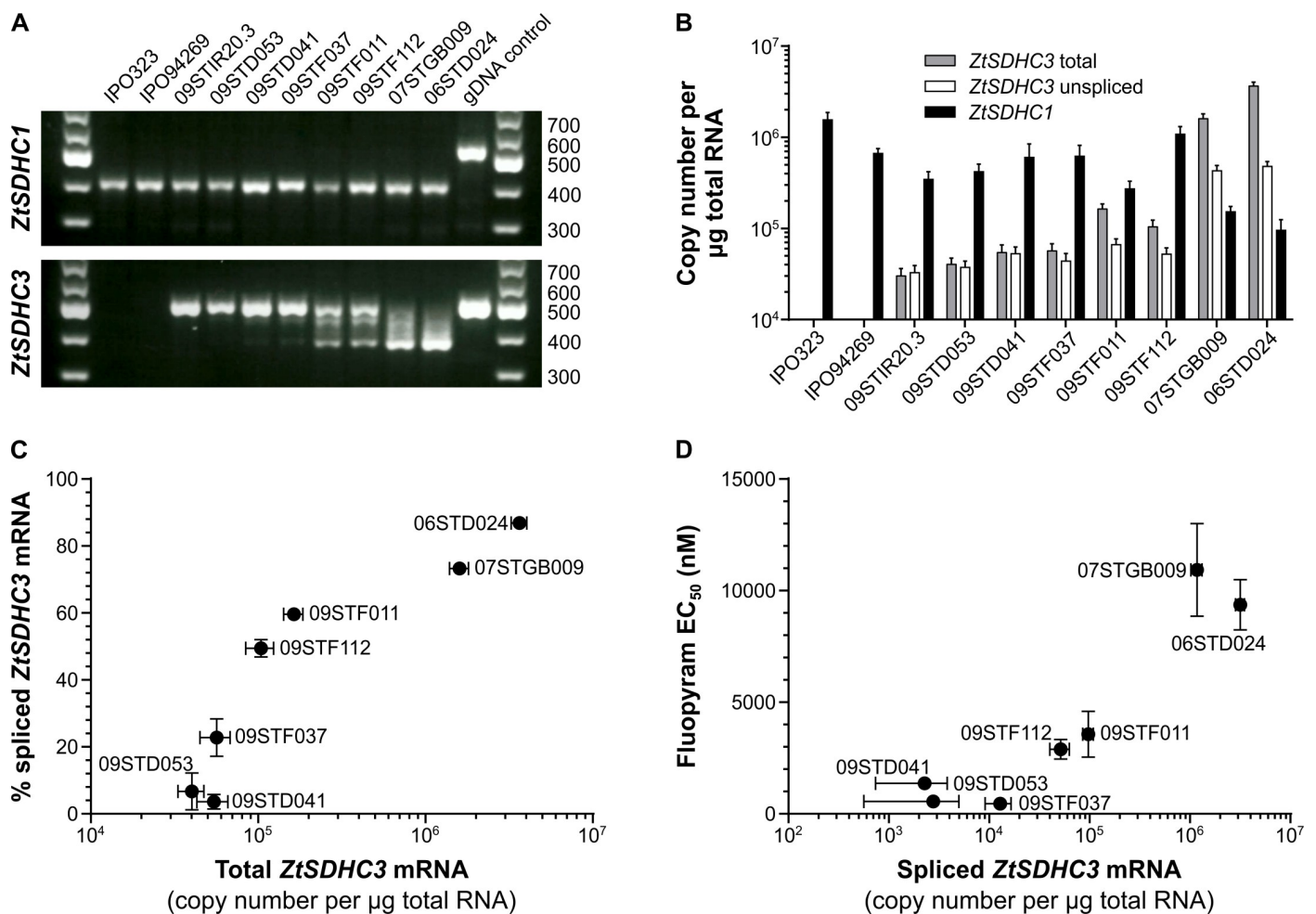
Fig 7. Fungicide sensitivity, gene expression and mRNA splicing in *alt-SDHC*-containing field isolates. (A) Gel electrophoresis of RT-PCR products of *ZtSDHC1* and *ZtSDHC3* (5' regions encompassing 2 introns each). gDNA of strain 06STD024 was used as control. Two control strains (IPO323 and IPO94269) lack the *ZtSDHC3* gene whereas the other eight isolates (09STIR20.3, 09STD053, 09STD041, 09STF037, 09STF011, 09STF112, 07STGB009 and 06STD024) all carry the gene. (B) Absolute quantification by hydrolysis probe RT-qPCR of total *ZtSDHC1* mRNA, and of total and unspliced *ZtSDHC3* mRNAs. Error bars correspond to standard deviation (± SD) corresponding to eight individual determinations. (C) Plot of total *ZtSDHC3* mRNA for each isolate versus calculated percentage of spliced *ZtSDHC3* mRNA. Results for strain 09STIR20.3 not displayed (calculation leading to negative value, S5 Dataset). (D) Plot of spliced *ZtSDHC3* mRNA against fluopyram sensitivity in liquid culture (EC$_{50}$ in nM). Vertical error bars correspond to the standard error of the mean (± SEM) corresponding to at least five individual determinations of fluopyram EC$_{50}$ (S5 Table). Results for strain 09STIR20.3 not displayed.

https://doi.org/10.1371/journal.ppat.1007780.g007

Overall, the quantity of spliced *ZtSDHC3* mRNA correlated with fluopyram resistance levels (Fig 7D and Table 3). Interestingly, *ZtSDHC1* expression levels were concomitantly found to be the lowest in the most highly *ZtSDHC3* expressing strains 06STD024 and 07STGB009 (Table 3 and Fig 7B), suggesting a possible link between the two.

At the protein level, the total amount of mitochondrial SDHC proteins (alternative and core) ranged between 21 fmol in IPO94269 to 134 fmol in 07STGB009 suggesting that the total amount of mitochondrial SQR protein varied across isolates (Table 3). Surprisingly, the alternative SDHC protein could be detected in all isolates carrying the gene, including the fully sensitive isolate 09STIR20.3 in which the alternative *ZtSDHC3* mRNA is very poorly expressed and for which splicing was not detected (Table 3 and Fig 7A). Isolates 06STGB009 and 07STD024 which showed the strongest fluopyram resistance also displayed the highest amount of alternative SDHC protein (up to 120 fmol in 06STGB009). These high levels of alternative SDHC protein were associated with very low (0.4 fmol in 07STGB009) or undetectable (in 06STD024) amounts of the "core" SDHC protein. Moderately tolerant isolates 09STF011 and 09STF112, in which balanced splicing of *ZtSDHC3* mRNA was detected, also displayed a balanced abundance of both SDHC proteins from 38.6 to 57.7 fmol for alternative alt-SDHC while the core SDHC protein was depleted but still detectable at 7.8 and 4.6 fmol respectively. Despite the differences in splicing efficiency, isolates 09STD041 and 09STF037 displayed very similar SDHC proteins quantities and ratios compared with 09STF011 and 09STF112. This was unexpected given the differences in RT-PCR suggesting lower quantities of the alt-SDHC protein should have been observed. Finally isolates 09STIR20.3 and 09STD053 for which no or very low *ZtSDHC3* mRNA splicing could be detected displayed amounts of core SDHC similar to WT isolates IPO323 or IPO94269. The alt-SDHC protein was detected at similar levels to other moderately or poorly shifted isolates in 09STD053 (48.6 fmol) and in much lower amounts in 09STIR20.3 (2.0 fmol) for which no splicing of the *ZtSDHC3* mRNA was detected.

These data demonstrate the importance of expression levels and splicing efficiency of *ZtSDHC3* mRNA in conferring the resistance phenotype. They also suggest that the alt-SDHC protein is more stable compared to the core SDHC in *Z. tritici* mitochondria, since very low expression of the functional spliced mRNA is sufficient for detection of the protein. Depletion of the core SDHC subunit, which is likely due to its replacement by alt-SDHC within the SQR enzyme, seems to correlate to the resistance phenotype.

Up-regulation of *ZtSDHC3* gene expression in field isolates is associated with transposons insertions in the promoter region

Comparing the *ZtSDHC3* locus of isolate 06STD024 to the corresponding locus in the 3D7 genome identified the insertion of a large class II transposable element (TE) (no cat element 8, 7 kb) [35], located 182 bp upstream of the *ZtSDHC3* start codon (Fig 2D). This DNA transposon was found at different genomic loci and in variable copy numbers among fully sequenced *Z. tritici* isolates. The presence of a TE in the promoter of the *ZtSDHC3* gene in our most SHA-SDHI tolerant isolate suggested that promoter variations may be responsible for the differences in expression and alternative splicing described above. Fragments encompassing the *ZtSDHC3* gene as well as ~1.5kb downstream and upstream sequences were amplified and sequenced in the eight isolates already characterized for fluopyram/SHA-SDHI resistance (Fig 7).

All isolates, except 07STGB009, displayed a similar *ZtSDHC3* locus organization to 3D7 (Fig 8A). SNPs, insertions and deletions were detected in the intergenic region located between *ZtSDHC3* and its 5' neighboring gene (EMBL: ZT3D7_G4529, Fig 8A). The highest variation in this region corresponded to a 23 bp deletion 80 bp upstream of *ZtSDHC3* start codon in moderately resistant isolate 09STF112.
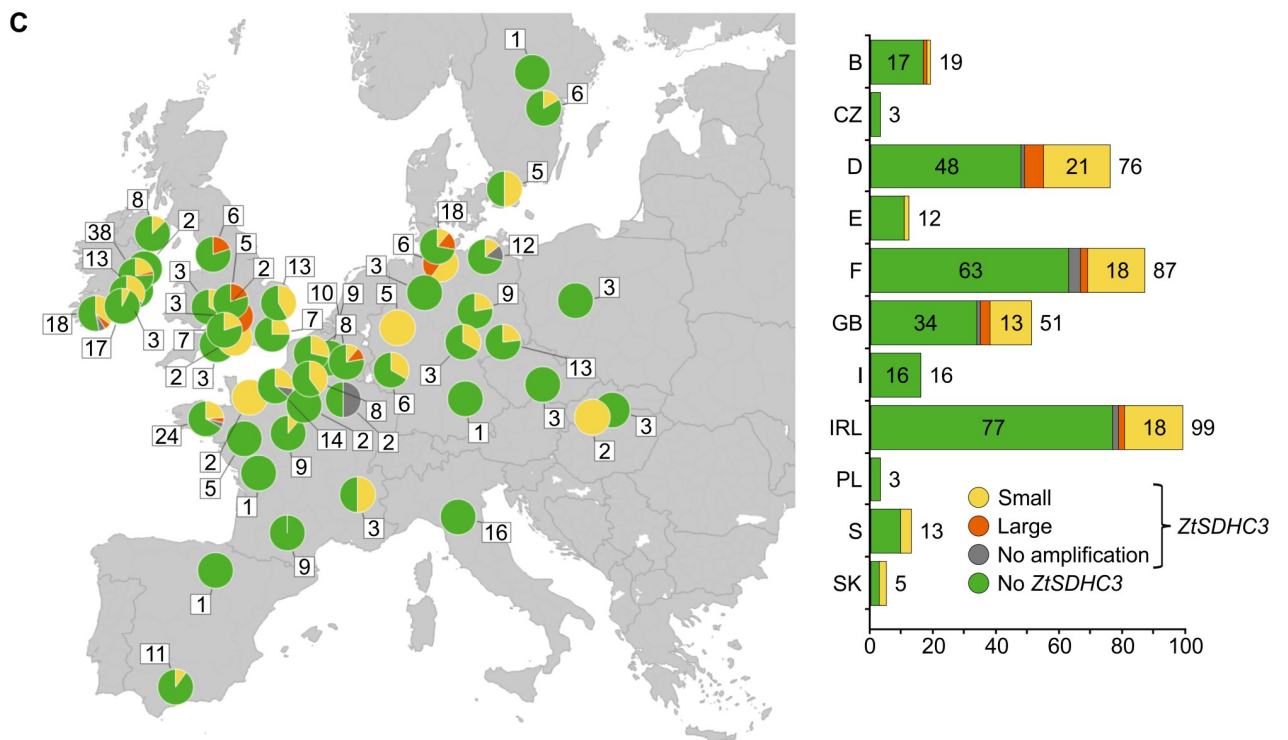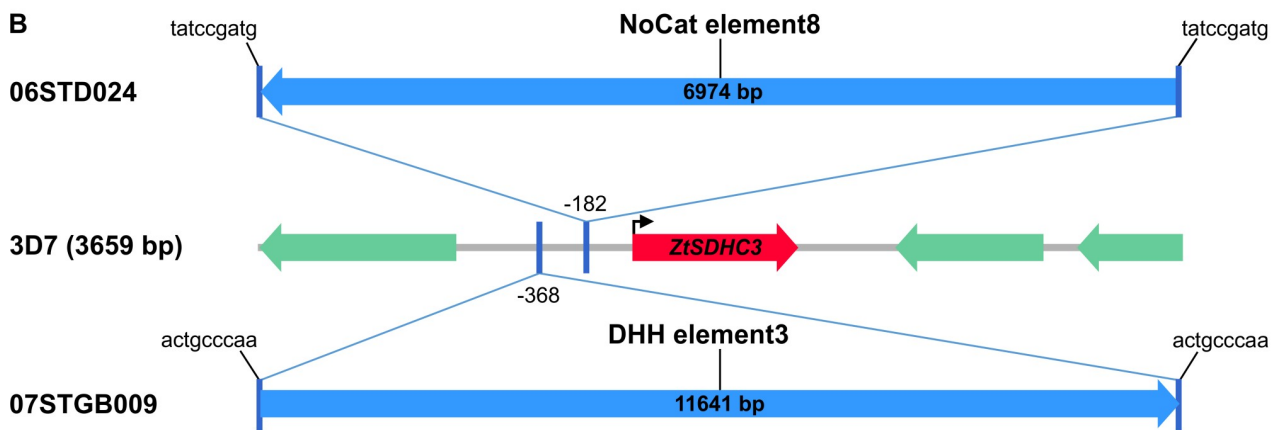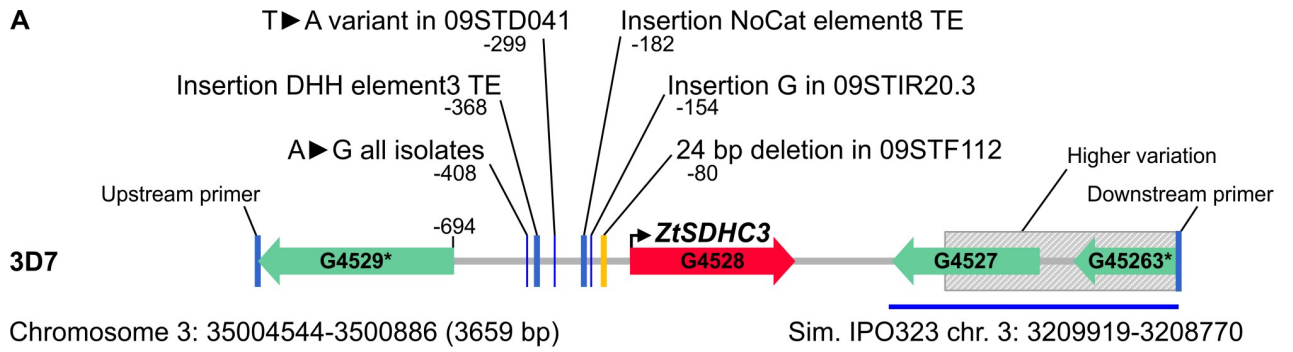
Fig 8. Structural variation at the *ZtSDHC3* locus in European *Z. tritici* field isolates and populations. (A) Structural overview of *ZtSDHC3* locus variations in a set of sequenced *Z. tritici* isolates. Mutations are lined up to 3D7 genomic structure, only mutations located within the region between ZT3D7_G4529 start codon to the stop codon of the *ZtSDHC3* gene are shown. Positions are numbered according to the *ZtSDHC3* start codon (+1). Sequences have been deposited at NCBI under references MK067275-MK067282. (B) Insertion of transposable elements in the promoter of *ZtSDHC3* of highly resistant 06STD024 and 07STGB009 field isolates. Target site duplications of 9 bp are flanking each transposon insertion. (C) European map with pie charts representing the 4 genotypes detected in *Zymoseptoria tritici* isolates collected in 2016. Green: *ZtSDHC3* gene absent, grey: *ZtSDHC3* gene present and no promoter amplification product, yellow: *ZtSDHC3* gene present and promoter of classical size, red: *ZtSDHC3* gene present and promoter of larger size. The total count of isolates for each sampling location is presented in white boxes. Right panel: Bar chart showing the total count of isolates of each type (similar color code) listed by countries.

Long range PCR was used to amplify a much larger fragment (12 kb) in the highly resistant isolate 07STGB009. In this isolate, we detected the insertion of a large class II DNA transposon of 11.6 kb in length and annotated DHH element 3 [35], in the promoter region of the *ZtSDHC3* gene (Fig 8B). This DNA transposon was also found at different genomic loci and in variable copy numbers among fully sequenced *Z. tritici* isolates. The transposon insertion site was located 368 bp upstream of the *ZtSDHC3* start codon and at 195 bp upstream of the other transposon insertion site in the 06STD024 strain. In both cases, a 9 bp sequence of the *ZtSDHC3* promoter was duplicated at the border of each transposon, suggesting the recent insertion of these transposons at these loci (target site duplication, Fig 8B) [39]. Overall the insertion of transposons in the promoter of *ZtSDHC3* was only observed in the two highly resistant isolates 07STGB009 and 06STD024. This result suggested that the insertion of transposons in the promoter of *ZtSDHC3* supports higher expression and better functional splicing of the gene.

Frequency of structural variants in *ZtSDHC3* promoter in European *Z. tritici* populations

In order to explore the frequency of structural changes in the *ZtSDHC3* promoter region at a population scale, a set of 145 strains carrying the *ZtSDHC3* gene and collected during the years 2009, 2010 and 2016 in Europe was assessed using locus-specific primers (S5 Table). Within this set of 145 field isolates, amplification products of 2.4 kb, similar to the expected size of 3D7, were obtained for 117 isolates (80.7%). Amplification products of larger sizes than 3D7, ranging between 3 and 20 kb, were found in 17 isolates (11.7%) and no amplification product was obtained for 11 isolates (7.5%). Insertion points were determined for 14 isolates displaying larger promoters (S8 Table). The insertion points ranged between 173 and 1073 bp upstream of the *ZtSDHC3* start codon, suggesting a wide range of structural variations. A graphical overview of the results obtained for the 2016 population (n: 387 isolates) characterized for presence/absence of *ZtSDHC3* gene and its promoter structure is presented on a graphical map of Europe (Fig 8C). The *ZtSDHC3* gene is widely distributed across Europe, but was more frequently found in isolates from the United Kingdom, Ireland and Northern regions of Germany and France. Structural promoter variants corresponding to potential insertions of transposons were detected in isolates from Germany, United Kingdom, Ireland, France and Belgium. Although tested isolates with insertions upstream of the *ZtSDHC3* gene being on average more resistant to fluopyram than isolates with no insertions (S4 Fig), the difference between the two groups was not statistically significant.

Discussion

A dispensable *SDHC* paralog is involved in resistance towards SHA-SDHIs

Baseline susceptibility survey of *Z. tritici* populations detected isolates resistant to SHA-SD-HIs, a novel subclass of SDHIs not previously used to control the disease. In this study we

show that SHA-SDHI resistance is governed by a single dispensable gene (*ZtSDHC3*) corresponding to a paralog of *SDHC* (*ZtSDHC1*), the gene encoding the C-subunit of the mitochondrial SQR enzyme. The deletion of *ZtSDHC1* in 06STD024, a field isolate carrying *ZtSDHC3* and highly tolerant to SHA-SDHIs, shows that the normally essential *ZtSDHC1* gene becomes dispensable in this genetic background. This result demonstrates that *ZtSDHC3* can compensate the function of *ZtSDHC1* and the strain-dependent essentiality of a gene of the core genome of *Z. tritici*. Similar examples of strain-dependent essentiality are likely to be identified among the core set of 9149 genes identified in the pangenome of this species [38]. The *ZtSDHC3*-dependent essentiality of the *ZtSDHC1* gene in *Z. tritici* populations may be a factor supporting its faster adaptive evolution [40]. This would match the observation that SDHI resistance mutations are mainly found within the *ZtSDHC1* gene in this species [17].

Phylogenetic analysis identified another *SDHC* paralog, *ZtSDHC2*, present in all sequenced isolates. This gene may result from an ancient duplication of the *ZtSDHC1* gene in a common ancestor of *Zymoseptoria spp.*, *Ramularia collo-cygni* and *Mycosphaerella emusae*. Functional studies will be necessary to assess whether this gene can perform a true SQR function. Available expression data suggest very poor expression of *ZtSDHC2* in characterized isolates (S3 Fig) [36, 41], but expression variants may exist in the population which potentially may confer novel target-based SDHI sensitivity patterns in this species and other pathogens carrying similar *SDHC* paralogs. Our work will therefore trigger further attention in an effort to understand resistance profiles displayed by strains that are deviating from the canonical SDHI sensitivity profile expected from their respective SDH subunits encoding genes.

Functional analysis of a simple alanine to isoleucine substitution supports the fine elucidation of binding interactions across commercial SHA-SDHIs

Despite the low similarity between SDHC and alt-SDHC proteins (62%), we show that a single isoleucine at position 78 within the alt-SDHC protein, a position corresponding to alanine 84 in SDHC, is mediating resistance towards SHA-SDHIs. SHA-SDHIs are differently affected by the mutation with an effect on enzyme inhibition ranging between complete loss of inhibition, with resistance factors over 20'000 fold for isofetamid, to only 6 fold resistance for pydiflumetofen (Table 1). These contrasting effects were well reflected *in vivo* and *in planta*. The presence of the *ZtSDHC3* paralog in *Z. tritici* populations has therefore major practical consequences for commercialized molecules of this class. In this study, we demonstrate maintained control of highly SHA-SDHI tolerant isolate by pydiflumetofen. Another study reported practical resistance towards isofetamid (and fluopyram) in highly SHA-SDHIs tolerant isolates [21]. We describe at an atomistic level the reasons for differential potency and cross-resistance among commercial SHA-SDHIs using docking simulations in the 3D models of the two SQR-enzymes (SDHC, alt-SDHC). Our simulations match the observations since isofetamid is found to be incompatible with the smaller binding pocket caused by isoleucine 78 of alt-SDHC. Conversely, pydiflumetofen is predicted to adopt a conformation that is, in its energy minimum, compatible with alt-SDHC SQR binding. The detailed features of pydiflumetofen binding were explained by the comparative assessment of matched pairs analogs on the two SQR enzymes and provide clues for the rational design of novel potent SDHIs not affected by mutations at the alanine 84 position of SDHC. This information is particularly relevant because *Phakopsora pachyrhizi* the causal agent of Asian soybean rust and a primary target for disease control, has recently developed resistance towards commercial SDHIs by the acquisition of an I86F mutation in the SDHC subunit, a position corresponding to A84 in *Z. tritici* SDHC [42].

A competition between SDHC and alt-SDHC proteins for functional integration into the mitochondrial SQR enzyme influences resistance levels

The characterization of the abundance of the two proteins (SDHC, alt-SDHC) in mitochondrial extracts shows that the SHA-SDHIs resistance is not only associated to the presence of higher levels of the alt-SDHC protein but also to a reduced abundance of the SDHC protein (Table 3 and S5 Fig). This observation is reflecting the competition between the two C-subunits proteins (alt-SDHC and SDHC) for functional integration in the SQR complex (S5 Fig). The outcome of this competition leads to mixed populations of the two types of SQR enzymes which are simultaneously present and functional in the mitochondria of a same isolate. We show that SQR enzyme composition impacts resistance levels *in vitro* and *in vivo* (Tables 1 and S5 and S5 Fig), which is in full agreement with our previous observations using the expression of a mutated form of the *SDHB* gene in a WT background [14].

Variation in resistance levels across field isolates carrying the *alt-SDHC* gene is due to polymorphisms in expression and alternative splicing

Characterization of *Z. tritici* field populations for the presence / absence of the *alt-SDHC* gene shows that 20 to 30% of the EU population carries the paralog. However, highly variable SHA-SDHIs resistance levels are observed among these isolates which is associated with differences in *ZtSDHC3* mRNA expression and its alternative splicing. We observe that, in the panel of studied isolates, a high level of *ZtSDHC3* expression globally correlates with increased splicing efficiency and resistance to SHA-SDHIs. However, using pTet::*SDHC3* transformants similar splicing efficiencies are observed at both high and low *ZtSDHC3* expression regimes (S5 Fig). This result is suggesting that strain-specific mechanisms are involved in the differential splicing efficiency observed among field isolates. The alternative splicing of *ZtSDHC3* mRNA is intriguing since the two 56 bp introns of *ZtSDHC3* carry the expected canonical fungal donor and acceptor sites. Further work will be required to understand which sequence features of *ZtSDHC3* introns are involved in such alternative splicing events [43]. This topic is of relevant interest to provide information on the regulation of alternative splicing in fungi.

Transposons insertions in the promoter of *ZtSDHC3* is associated with high levels of resistance to SHA-SDHIs

The analysis of a large collection of 145 *Z. tritici* isolates show that most isolates carrying *ZtSDHC3* promoter insertions also display higher tolerance towards SHA-SDHIs (S4 Fig). The sequencing of *ZtSDHC3* promoter in two isolates displaying high SHA-SDHIs resistance levels evidenced transposons insertions close to the start codon of *ZtSDHC3*. The different nature of the two transposons and their different insertion sites, near the start codon of *ZtSDHC3* strongly suggest that they occurred independently during the evolution of the *Z. tritici SDHC3* locus. We hypothesize that these insertions are responsible for the high alt-SDHC protein expression levels observed in these isolates and their high resistance to SHA-SDHIs. Further validation by reverse genetics will be required to confirm this hypothesis. The molecular characterization of promoter insertions in other SHA-SDHIs-resistant isolates may therefore permit the discovery of additional mobile elements. In addition, the SHA-SDHIs sensitivity shift conferred by a *de novo* TE insertion in the promoter of a strain with low alt-SDHC protein expression may enable the selection of *de novo* insertions in directed evolution experiments [44]. As such the promoter of *ZtSDHC3* and cognate SHA-SDHIs resistance may constitute a valuable system for the study of active TEs in *Z. tritici*.

Role of *SDHC* subunit paralogs in fungi

The biological role of multiple *SDHC* paralogs in fungi is not known. Duplication of the *SDHC* gene occurred multiple times throughout fungal evolution, but the conservation (or loss) of the paralog(s) appears species-specific (S4 Table). We have looked at possible roles of this SDHC diversity.

A role for the presence of *SDHC* paralogs may be related to the occurrence of natural SDHIs produced by competing species. Indeed, siccanin (a metabolite from *Helminthosposium siccans*) and atpenins (metabolites from *Penicillium sp.*) inhibit bacterial, fungal and mammalian SQRs by binding to the same (Qp) site as synthetic SDHIs [45–47]. Metchnikowin, an antifungal peptide from *Drosophila melanogaster*, binds to the *Fusarium graminearum* iron-sulfur subunit SDHB and also inhibits fungal SQR *in vitro* [48]. Therefore, SDH inhibition by natural antifungal compounds could be a driving force for the selection of *SDHC* paralogs conferring resistance to these inhibitors in fungi. Similar mechanisms have been described in the evolution of bacterial resistance genes [49].

Another role could be linked to metabolic adaptation. Indeed, the presence of *SDH* subunits paralogs may allow the controlled production of hybrid SQR enzymes of different efficiencies which may represent an advantage under specific developmental or growth conditions as found in parasitic nematodes [50, 51], plants [52] and yeast [53, 54]. In yeast, one paralog of the SDHC subunit and one paralog of the SDHD subunit were shown to lead to hybrid functional SQR enzymes which, although less active, play a role in cell adaptation to specific environmental conditions [53]. These hybrid SQRs conferred "metabotypes" and growth yields very distinct from WT-SQR [53, 54]. Interestingly, the yeast *SDHC* paralog may also carry additional function(s) as a component of the TIM22 inner membrane translocase [55]. In *Z. tritici*, the alt-SDHC protein was still detected in the mitochondria of isolates that displayed very low expression of the *ZtSDHC3* mRNA. By contrast, the SDHC protein appeared fully degraded when not integrated into the SQR enzyme (Table 3 and S5 Fig). This suggests an additional function of the alt-SDHC paralog or reduced scavenging of the protein when not integrated in the SQR enzyme.

Practical consequences for disease control, resistance evolution and research for new active ingredients

Fluopyram is currently the only SHA-SDHI molecule registered for STB control in Europe. Since this fungicide does not control SHA-SDHIs resistant isolates *in planta* we expect a strong selection of isolates carrying the *ZtSDHC3* gene in fields treated by the solo compound [21]. However, fluopyram is sold as a mixture with another SDHI (bixafen), and an azole (prothioconazole) which are both effective on isolates carrying *ZtSDHC3*. Using a GM approach, we artificially generated isolates only carrying the altC-SQR enzyme which represents a worst case scenario for this paralog-mediated resistance mechanism. We observed that, despite the superior SHA-SDHI resistance displayed by the GM isolate (KO-*SDHC1*) compared to the original isolate, the dose of pydiflumetofen required for full *in planta* control was similar to that of other SDHIs on the market for controlling wild type isolates. Our results are therefore supporting the use of a robust rate for the novel SHA-type SDHI pydiflumetofen in order to secure an effective control of the whole population, including strains carrying the *ZtSDHC3* gene.

Although combining molecules with different modes of action is a method routinely used for STB control, yet it is likely that the use of SHA-SDHIs will exert a selection for strains carrying the *ZtSDHC3* paralog. The *ZtSDHC3* paralog we discovered will require further scrutiny since this gene may also acquire mutations leading to broad SDHI resistance. Furthermore, sequencing of the *ZtSDHC3* gene evidenced rare and potentially functional variants of the alt-

SDHC protein. Among the variants, the alt-SDHC_S86Y mutant shows a mutation at a Qp site position homologous to serine S83 in SDHC, whose substitution to a glycine conferred resistance towards a broad range of SDHIs in laboratory mutants [14]. The only well described example of a fungicide target paralog driving resistance evolution comes from *Rhynchosporium commune*. In this species, the *CYP51A* gene, a paralog of CYP51 the target of azole fungicides, was mostly absent in populations before introduction of azoles. This paralog re-emerged following the adoption of azole fungicides and recently acquired non-synonymous mutations, two events which are driving the azole fungicides sensitivity shift in this species [56, 57].

The presence of the *ZtSDHC3* paralog in *Z. tritici* populations may support a higher adaptive evolution of *ZtSDHC1* since we show that in some genetic backgrounds, this paralog can functionally substitute *ZtSDHC1* in its essential SQR function. Whether *alt-SDHC* will become a primary driver for SDHIs resistance evolution in *Z. tritici* remains to be seen. Our current view is that SDHI resistance in *Z. tritici* will continue to be driven by mutations in the core *SDH* genes because (i) the *ZtSDHC3* gene only represents an advantage for the SHA subclass of SDHIs and because (ii) the amplitude of the resistance phenotype conferred by *ZtSDHC3* is limited by its competition with the core SDHC for inclusion in the SQR complex [17, 18]. The gained awareness on the potential influence of *SDH* genes paralogs in driving SDHIs sensitivity shifts will support a more systematic assessment of potential expression variants in tolerant isolates of *Z. tritici* and other species.

Our findings show the importance of analyzing fungal populations and determining the mechanisms involved in fungicide sensitivity variation during the AI optimization phase. The decreasing cost of population-wide genome sequencing and the widespread adoption of genome-wide association studies (GWAS), should facilitate the identification of the molecular factors involved in baseline fungicide sensitivity [33, 58]. Since the increased natural variation encompassed by paralogs provides a source of direct adaptation to natural compounds or xenobiotics, it is likely that population genomics studies will enable the discovery of additional dispensable paralogs of fungicide targets or detoxification genes. For agrochemical research, population variation is a major challenge that needs to be addressed and an in depth understanding of the molecular mechanisms affecting sensitivity to fungicides represents a real opportunity for more accurate chemical design.

Materials and methods

Strains, media and culture conditions

All *Z. tritici* strains were isolated from infected wheat leaves collected during Syngenta European monitoring following already described procedures [22]. The reference strains IPO323 and IPO94269 were kindly provided by Gert H.J. Kema (Wageningen University, NL). The isolates were inoculated from stocks stored in liquid nitrogen onto solid V8 agar at 18°C for 5 days [59]. Fresh cells were harvested from these plates and used as an inoculum for all experiments. The following media were used throughout: TSM40 (4 g.L^{-1} glucose, 10 g.L^{-1} malt extract, 4 g.L^{-1} yeast extract, pH 7.0); AE medium [60]; induction medium (IM) [59], YPD (10 g.L^{-1} yeast extract, 20 g.L^{-1} peptone, 20 g.L^{-1} glucose). DH5α, TOP10 or DB3.1 cells (Invitrogen) were used for the maintenance of plasmids in *Escherichia coli*. *Agrobacterium tumefaciens* strain EHA105 [61, 62], was used for *A. tumefaciens* mediated transformation (ATMT) following procedures described in [59].

Liquid culture assays for fungicide sensitivity determination

Pre-culture of the inoculum and fungicide sensitivity tests were performed following previously described procedures [14]. Different ranges of inhibitor concentrations were used for

population monitoring and for the detailed phenotyping of a selected set of individual field isolates and genetically modified strains. For fungicide sensitivity monitoring of European field populations, final inhibitors concentrations were between 100 mg.L^{-1} and 0.0001 mg.L^{-1} with uniform 10x dilution steps (7 inhibitor concentrations + DMSO control). For refined sensitivity analysis of a smaller panel of isolates final inhibitor concentrations ranged between 0.5 mM and 0.47 nM with uniform 4x dilution factor steps (11 inhibitor concentrations+ DMSO control).

Mapping population generation and resistance mapping

Mating type determinations were performed using PCR markers described in [63]. 06D024 x IPO323 and 07GB009 x IPO94269 crosses were performed as previously described in [64]. Single ascospore progeny isolates were collected and groups of 234 and 96 isolates were obtained respectively. Fluopyram resistance inheritance was determined by spotting 2μl of 2.10^6 cells. ml^{-1} onto AE agar supplemented or not with fluopyram 10 mg.L^{-1}. DNA extraction were performed using fresh culture grown on V8-agar plates (5 days, 18°C in the dark), approximatively 100 mg of fresh cells were collected with an inoculation loop and processed to DNA extraction using the DNeasy 96 Plant Kit (Qiagen) and following provider's instructions. For pool sequencing, 2 μg of DNA for each pool was sheared to an average fragment size of 340 base pairs using a Covaris S220 focused-ultrasonicator (Covaris, Inc., Woburn, Massachusetts, USA). The samples were then cleaned using DNAClean XP (Beckman Coulter Life Sciences, Indianapolis, Indiana, USA). Sequencing libraries were prepared from the sheared DNA using the NEBNext DNA library prep kit for Illumina (New England BioLabs, Ipswich, Massachusetts, USA). Size selection was performed using an E-gel precast agarose system. Each sample was run in three lanes of an Illumina Genome Analyzer II (Illumina, San Diego, California, USA) in a 36 cycle paired end run. Total sequence yield was 2.7 gigabases for the resistant pool sample and 3.3 gigabases for the susceptible pool. Sequence reads were aligned to the JGI *M. graminicola* v2.0 assembly, using gsnap [65] and uniquely aligning reads were used to call variants with the Alpheus pipeline [66], with filtering criteria requiring at least 2 reads having average base quality of ≥ 20 with an allele frequency within the sample of ≥ 0.2. Differences in allele frequencies between the pools were then used to determine the putative genomic location of the causative variants. All PCR-based genotyping assays (SSR, CAPS) were run on individual genomic DNA using GoTaq DNA polymerase, at recommended temperature and cycling parameters and using oligonucleotides and enzymes listed in S7 and S1 Tables respectively.

Phylogenic analysis of fungal SDHC proteins

Orthologs for ZtSDHC1 were retrieved using ENSEMBL ortholog/paralog prediction where available [67]. For *ZtSDHC2* and *ZtSDHC3* or genomes in which no orthologs were mapped in ENSEMBL a reciprocal BLAST was performed to identify homologous sequences. All retrieved sequences were run through TargetP analysis [34] and only mitochondrially targeted sequences were retained. Sequences were aligned using Clustal-omega with default settings [68]. A tree was drawn using PhyML for amino acid sequences using the best of NNI and SPR as the tree topology search operation (LogLk = -21960.63386) [69]. The tree was visualized using iTOL [70].

PCR methods and Sanger sequencing

All oligonucleotides were purchased from Microsynth AG (Balgach, 175 Switzerland). PCR primers used to amplify sequences for CAPS/SSR markers, Sanger sequencing or clonings are

listed in S4 Dataset. PCR products for cloning or direct Sanger sequencing were obtained using the Phusion Hot Start II High-Fidelity DNA Polymerase (ThermoFisher Scientific, F549L). For the long PCR products required to characterize promoter inserts, LongAmp Taq DNA Polymerase (NEB, M0323S) was used. PCR products for classical genotypings such as CAPS markers or SSR analysis were amplified using GoTaq G2 Hot Start Polymerase (Promega, M7405). Each PCR was performed according to the conditions recommended by the respective manufacturers. Sanger sequencing was done at Microsynth AG (Applied Biosystems 3130 Genetic Analyzer). Pyrosequencing was performed on a PyroMark Q96 ID (Biotage/QIAGEN).

DNA was extracted using the DNeasy 96 Plant Kit (Qiagen) following provider's instructions. For the sequencing of large promoter insertions, the large fragments were cloned into TOPO vectors and a primer walking procedure applied at Microsynth AG (Balgach, 175 Switzerland).

Growth tests on solid agar at discriminatory fungicide concentrations

A large scale spotting assay of 96 isolates (Fig 6) was performed using the V&P 96 floating pin tool VP408FP6 (V&P Scientific), equipped with flat tip FP6 pins of 1.58 mm diameter (resulting in approx. 0.4 µl transfer volume). Source cultures for cell spotting were grown in 100 µl YPD liquid medium in a 96 well flat bottom plate (Corning, 3370) at 18˚C for 11 days (average cell density of $3.5 \cdot 10^6$/ml), then diluted 1:2x in fresh YPD medium and incubated for another 1.5 h before transfer with the pin tool (approx. 700 cells per spot) onto AE agar with or without fungicide. Plates were incubated at 20˚C in the dark for up to 18 days. Smaller scale spotting assays (Figs 4 and 8) were performed using 5 days V8-agar plates inoculums adjusted to 2.10^6 spores.mL^{-1} in water and diluted in steps of 3. 2µL of spore suspension was spotted on the plates, and the plates were incubated shielded from light at 21˚C for 6 days.

In planta fungicide dose response

Wheat (*Triticum aestivum*) variety Riband was grown in pots (d = 6.5cm), at a density of 4 plants per pot and treated with the growth regulator CCC (Chlorcholinchlorid; Chlormequat; 5 ml / pot, 0.4% solution) 4 days after sowing. Wheat plantlets were maintained in a climatic room at 18˚C, 60% humidity and under a 12h light regime (high intensity). Fungicide applications were performed on 14 days old plantlets for which leaf 2 is the fully expanded target leaf. Fungicide treatments were performed using a custom-made track sprayer adjusted at 200L.ha^{-1} (Nozzle: Lechler, orange LU90-01). The fungicides used were Solatenol EC100 (Elatus Plus, benzovindyflupyr), Isopyrazam EC125 (Seguris Flexi or Reflect), Adepidyn EC100 (research formulation of pydiflumetofen). *Z. tritici* infections were performed using a Devilbis airbrush (spray of about 150ml.m^{-2}) one day after fungicide application and using an inoculum grown on V8-agar adjusted to $1.8.10^6$ spores.ml^{-1} in 0.05% Tween20 in MQ water. Inoculated plants were initially incubated for 72h under reduced light conditions and high humidity using towel-covered Plexiglas hoods in a climatic chamber set to 21˚C/19˚C day/night alternations, 80% humidity and a 14h light regime. The Plexiglas hoods were then removed until evaluation. Plants were fertilized once per week and disease evaluation performed based on disease coverage on the second leaf approximately 16–19 days after infection, once untreated plants reached 75–90% disease coverage. Each fungicide was tested at several rates to produce dose responses. There were 3 pots (4 plants each) per fungicide rate and isolate, the whole experiment was repeated 4 times. *In planta* EC$_{50}$ were calculated using the software GraphPad Prism v6.08.

Production of *Z. tritici* transformants

The multisite binary pNOV2114_gateway and pNOV2114 Hyg _gateway (3-way) vectors were used to generate the different transformation constructs [14]. To generate the *SDHC1*

and *SDHC3* KO mutants, 5' upstream regions of 1000bp and 2074 bp and 3' downstream regions of 914bp and 1313bp for *ZtSDHC1* and *ZtSDHC3* respectively were PCR-amplified from genomic DNA of IPO323 or 06STD024 strains and the fragments cloned by BP cloning using Gateway BP Clonase II Enzyme Mix (Invitrogen) into pDONR-P4-P1R (upstream regions) or pDONR-P2R-P3 (downstream regions) (S4 dataset for oligos). These 5' and 3' gene locus-paired entry plasmids were then combined with the pENTR221-TrpChyg described previously [59] and pNOV2114_gateway for multisite gateway LR cloning using Gateway LR Clonase II Plus enzyme Mix (Invitrogen) following provider's instructions. The final pNOV2114 KO-SDHC and pNOV2114 KO-alt-SDHC binary plasmids carry a hygromycin resistance cassette flanked by 5' and 3' upstream regions of the *ZtSDHC1* and *ZtSDHC3* genes respectively.

For generating expression constructs under the control of a tetracyclin-repressible promoter, the plasmid pMF2-4h [71] was modified by removal of the hygromycin resistance cassette after digestion by *NotI* and recircularization of the plasmid to generate pMF2-4h⁻. The fragment containing the full Tet repressor expression cassette followed by operator sequences fused to *MfaI* minimal promoter was PCR amplified from re-circularized pMF2-4h⁻ plasmid and cloned by gateway cloning into pDONR_P4P1R using oligos listed in S4 dataset.

To generate the *SDHC3* expression plasmids, the *ZtSDHC3* gene of 06STD024 was amplified from the genome and cloned into pDONRZeo by gateway cloning to generate pENTR-Zeo-alt-SDHC. A variant of this plasmid (pENTRZeo-alt-SDHC_I78A) encoding the I78A variant of *alt-SDHC* was obtained by site-directed mutagenesis using QuikChange II Site Directed Mutagenesis kit (Stratagene) following provider's instructions and oligos listed in S4 dataset. The Tetoff promoter region from plasmid pMF2-4h [71] was sub-cloned into pDONR221 using oligos listed in the S4 Dataset. These entry plasmids were combined with pENTR_TrpCterm and pNOV2114 Hyg_gateway plasmids [59] to generate the pNOV2114_-Tetoff_alt-SDHC_TrpCterm and pNOV2114_Tetoff_alt-SDHC^I78A_TrpCterm binary vectors used for transformation of IPO323.

All entry and subsequent binary plasmids were validated by Sanger sequencing of the cloned fragment before transfer to *A. tumefaciens*. *Z. tritici* transformation was performed as described previously [59]. *Z.tritici* transformants were validated by PCR using primer combinations enabling the validation of successful gene deletion events for the KOs mutants or the completeness of the transformation cassette for the ectopic expression mutants.

Quantitative Real-Time PCR and semi-quantitative PCR

To produce the RNA samples, field isolates and transformants were initially inoculated on V8-agar plates and left to grow for 4 days, 25 ml TSM40 liquid cultures in 100 ml round bottom Erlenmeyer flasks were then initiated using 10 μl inoculation loops. The flasks were incubated at 20˚C, 160 rpm, for 4 days before cells were harvested by filtration using a tissue filter and ground in liquid nitrogen using mortar and pestle. For RNA extraction, 50 mg of the powdered material was processed with the RNeasy Plant Mini kit (Qiagen, 74904) according to the manual and including an on-column DNase I digestion (Qiagen, 79254). A second DNase digestion was performed on the eluates, followed by purification using the same RNeasy Plant Mini kit. RNA yield and integrity was determined on an Agilent 2100 Bioanalyzer System and the absence of residual genomic DNA in the samples was verified by PCR, using primers specific for the β-tubulin (*TUB1*) gene (S4 Dataset) and the cycling protocol described below for semi-quantitative PCR. The High Capacity cDNA Reverse Transcription kit (Applied Biosystems, 4368814) was used for reverse transcription of 2 μg of total RNA per sample, using the RT Random Primers provided in the kit and according to the manufacturer's instructions.

Semi-quantitative PCR was performed using GoTaq G2 Flexi DNA Polymerase (Promega, M7805) and the PCR primers listed in (S4 Dataset). *ZtSDHC1* and *ZtSDHC3* from field isolates and reference strains were amplified from undiluted cDNA, whereas cDNA for detection of the β-tubulin sequence *TUB1* and of the *ZtSDHC3* expression strain (samples pTet::*SDHC3* and pTet::*SDHC3* + Dox) were diluted 1:3x in water before use. Genomic DNA of isolate 06STD024 was included as control (carrying un-spliced template sequences for all three targets). The PCR program was: Initial denaturation for 2 min at 95˚C, followed by 40 cycles of denaturation at 95˚C for 30 s, primer annealing at 54˚C for 30 s and extension at 72˚C for 34, followed by a final incubation for 5 min at 72˚C.

Quantitative Real-Time PCRs were performed with all four targets in a multiplexed reaction using hydrolysis probes carrying different fluorophores and quenchers listed in S4 Dataset. The binding sites of qPCR oligonucleotides within *ZtSDHC1* and *ZtSDHC3* are shown in S6 Fig. Primers were used at 900 nM and hydrolysis probes at 200 nM final concentration in 20 μl multiplexed qPCRs with KAPA Probe Force qPCR Master Mix 2x (Kapa Biosystems, KK4301) and 5 μl template DNA per well. The cDNA preparations were diluted 1:9x in DEPC-treated water immediately before the experiment. RNA (No-Reverse-Transcription reaction controls) of the same samples were also tested in two separate runs using the corresponding plate layout.

To enable absolute quantification, a reference plasmid was generated by the sequential cloning of the coding sequences of *ZtSDHC1*, *TUB1* (both amplified from cDNA of IPO323), and *ZtSDHC3* (from gDNA of 06STD024) using a GENEART Seamless Cloning and Assembly Kit (Invitrogen, A13288) and PCR oligos listed in S4 Dataset. The cloned fragments encompass the binding sites of the qPCR oligonucleotides. The resulting plasmid pUC19_cSDHC1_gSDHC3_cTUB1 (calculated molecular weight: 3200964.1 Da) was used to generate standard curves for both calculation of primer efficiencies and the absolute quantification of *SDHC1* and *SDHC3* copy numbers. A serial 1:6x dilution of pUC19_cSDHC1_gSDHC3_cTUB1 was made in 4 replicates, with a starting concentration of 4 pg/μl (resulting in 1 pg/μl or 20 pg total in the final reaction mix, 1 pg equals 188131 molecules based on the calculated molecular weight of 3200964.1 Da).

All 12 cDNA samples, a no-template RT reaction control and the reference plasmid dilution series were run on the same 96-well assay plate, with 4 technical replications per plate and the run was repeated on a duplicate plate. The qPCR was performed on a CFX96 Real-Time System on top of a C1000 Touch Thermal Cycler (Bio-Rad), and analyzed using the CFX Manager 3.0 software (Bio-Rad). The PCR program was: Initial denaturation for 3 min at 98˚C, followed by 45 cycles of denaturation at 95˚C for 10 s and combined annealing/extension for 20 s at 60˚C with subsequent plate reading. Assay results were exported to RDML format (S5 Dataset). For relative expression level comparisons of *ZtSDHC1* and *ZtSDHC3*_total/un-spliced the Starting Quantity (SQ) values of individual wells were used to calculate the respective copy numbers using the reference plasmid standard curves. Statistical analysis was then performed on the 8 technical replicate values from individual wells.

Mitochondria isolation and enzyme assays

Biomass production, mitochondrial extraction and purification were performed as described in [14]. Succinate: ubiquinone/DCPIP sensitivity tests were performed as described in [14] with minor modification. The different mitochondrial suspensions were adjusted to similar initial velocity (1 OD_{595nm} hour^{-1}) and inhibitor concentrations ranged between 0.047nM and 50μM with uniform 4x dilution steps (11 concentrations + DMSO control). Calculated

absorbance slopes (OD/min) were used for IC50 calculations using GraphPad Prism 6.07 software non-linear curve fitting against log inhibitor concentrations.

Sample preparation for SDHC and alt-SDHC protein quantitation

Protein from mitochondrial extracts was precipitated using trichloroacetic acid/acetone. After resuspension under denaturing conditions, the total protein concentration was estimated using a Bradford assay [72]. An aliquot of 25 μg protein from each sample was separated on a 10% NuPAGE gel (Life Technologies). Gels were stained with colloidal Coomassie blue, and a gel region (10–25 kDa) from each lane was excised for trypsin digestion. In-gel digestion was carried out using a published protocol [73]. After digestion, peptide samples were dried using a centrifugal evaporator, and re-suspended in LC-MS/MS sample buffer containing 3% acetonitrile, 0.1% formic acid, 100 femtomole (fmol) per microliter isotopically labelled internal peptide standards (JPT Peptide Technologies GmbH, Berlin, Germany). Peptide sequences and isotopic labelling information can be found in S7 Table. The peptides used for the LC-MS/MS analysis were chosen based on sequence uniqueness in the *Z. tritici* proteome. The peptides had also been identified in a separate proteomic analysis of mitochondrial extracts. Four technical replicates for each strain were prepared for LC-MS/MS analysis.

Multiple reaction monitoring LC-MS/MS analysis

LC-MS/MS analysis was done using a TSQ Vantage triple quadrupole mass spectrometer equipped with a nano-electrospray source (Thermo Fisher Scientific, Waltham, MA, USA) and coupled to an Ultimate/ Switchos split-flow LC system (Dionex, Thermo Scientific). A volume of 2.5 μl of each peptide sample was injected into the system. Peptides were separated on a Picotip column (75 μm, 15 cm column packed with 5 μm C18 particles; Nikkyo Technos Co., Ltd. Japan). Gradient elution was performed using 0.1% formic acid in water as solvent A and 99.9% acetonitrile/0.1% formic acid as solvent B. Gradient length was 30 min, from 3 to 40% solvent B. The flow rate was 300 nL per min. The TSQ Vantage instrument was operated with a capillary temperature of 275°C and spray voltage set to 1.7 kV. The data were acquired in positive scan mode with the collision gas set to 1.5 mTorr. The Q1 and Q3 peak widths (FWHM) were set to 0.2 u and 0.7 u, respectively. The cycle time was set to 5 seconds. No retention time scheduling for the two peptides was used. The list of monitored transitions and collision energy settings can be found in S8 Table. The run order of samples was randomised. The mass spectrometry raw files were imported into Skyline v1.2 software (University of Washington, USA). Integrated peak areas were exported to Microsoft Excel. The amount of SDHC and alt-SDHC protein in femtomole (fmol) was calculated based on the peak area for the endogenous peptide and the corresponding isotopically labelled internal peptide standard.

Homology model, docking simulations and conformational analysis

The homology model for *Z. tritici* WT-SQR with the "core" SDHC was generated as described in [14]. The homology model of the alt-SQR carrying the alternative SDHC subunit was generated following a similar procedure. Isofetamid, pydiflumetofen and compounds 1–3, were manually docked into the *Z. tritici* SQR Qp binding site. Interactions of key residues were determined through pharmacophore elucidation [14]. In a second step the protein ligand complexes were minimized using Moloc MAB force field [74], allowing full flexibility for the ligands while keeping the *Z. tritici* SQR protein rigid. For pydiflumetofen conformational analysis, a diverse set of 30 conformations were generated with the CCDC conformer generator [75]. Each conformation generated by the CCDC conformer generator was optimized with the M06L DFT [76] functional method and 6-31G(d) as basis set within Gaussian09 [77].

Additional parameters that were used: scrf = (iefpcm,solvent = water). Conformations have been evaluated based on the calculated DFT energy.

Supporting information

S1 Fig. Structure of carboxamides SDHIs molecules used in the study. Shaded grey area represents the SHA cross-resistance group. Schematic view of a typical SHA compound is shown in the bottom right corner.
(PDF)

S2 Fig. Phylogenic tree of fungal SDHC proteins. Tree generated using PhyML and visualized using iTOL (see material and methods). ZtSDHC1-3 paralogs are highlighted in yellow.
(PDF)

S3 Fig. Box plot of IPO323 time course expression of SDH-encoding genes. Expression data inferred from RNAseq (Rudd et al., 2015).
(PDF)

S4 Fig. Box plot of fluopyram sensitivity of 133 *Z. tritici* isolates collected in Europe in 2016. Isolates were grouped by genotyping based on the detection of the *ZtSDHC3* gene and *SDHC3*-promoter insertions. *ns: No significant difference in student t-test.
(TIF)

S5 Fig. Expression-driven competition of SDHC and alt-SDHC proteins for functional integration in the mitochondrial SQR. (A) RT-PCR analysis of *SDHC1* and *ZtSDHC3* in 06STD024 and IPO323 pTet:*SDHC3* transformant. The expected PCR products corresponding to fully spliced mRNAs were 389 and 384 bp for *ZtSDHC1* and *ZtSDHC3* respectively. (B) Absolute quantification by RT-qPCR of the three *SDHC* mRNA species in the 06STD024 strain and IPO323 pTet::*SDHC3* transformant. (C) Normalized proportion of the three mRNA species (as deducted from panel B). (D) LC-MS/MS quantification of the SDHC and alt-SDHC proteins in mitochondrial extracts from 06STD024 and IPO323 pTet::*SDHC3* transformant. Values presented are the mean of 6 individual experiments ± SD.
(TIF)

S6 Fig. Schematic view of oligo positioning for *ZtSDHC1* and *ZtSDHC3* Taqman RT-qPCR assays. Exons are shown as blue arrows and introns as grey bars, labelled hydrolysis probes are shown in red, forward and reverse PCR oligos are shown as black arrows. Oligonucleotides sequences and probe details are shown in S4 Dataset.
(TIF)

S1 Table. IPO323x06STD024 progeny genotyping results inferred from CAPS and SSR assays.
(XLSX)

S2 Table. IPO323 genes within the final 16 kb mapping window.
(XLSX)

S3 Table. 07STGB009xIPO94269 progeny genotyping results inferred from CAPS and SSR assays.
(XLSX)

S4 Table. Count of SDHC paralogs per species.
(DOCX)

S5 Table. Liquid culture SDHIs sensitivity for the panel of *Zymoseptoria tritici* field and genetically modified strains referred in the study. Mean: mean EC_{50} in nM, SEM: standard error of the means, N: number of individual determinations.
(XLSX)

S6 Table. Overview of *ZtSDHC3* sequencing and promoter PCR results for a panel of 154 isolates carrying the gene and collected in Europe in 2009, 2010, 2011 and 2016.
(XLSX)

S7 Table. Internal peptide standards used in the LC-MS/MS assay to quantify SDHC and alt-SDHC proteins.
(XLSX)

S8 Table. Monitored transitions in LC-MS/MS assay for quantifying SDHC and alt-SDHC proteins. The assay used a multiple reaction monitoring approach on a TSQ Vantage triple quadrupole mass spectrometer.
(XLSX)

S1 Dataset. Core *SDHB*, *SDHC* and *SDHD* genes sequencing results for a set of *Z. tritici* field isolates referred in the study. Base count according to first codon.
(XLSX)

S2 Dataset. Pool seq genotyping results and mapping interval.
(XLSX)

S3 Dataset. SDHC haplotypes (CDS and protein) for 350 EU *Z. tritici* isolates collected in 2016.
(XLSX)

S4 Dataset. Oligonucleotides used in the study.
(XLSX)

S5 Dataset. q-RTPCR results files in RDML format.
(ZIP)

Acknowledgments

Author Contributions

Conceptualization: Helge Sierotzki, Gabriel Scalliet.

Data curation: Stephanie Widdison, Grace Logan, Gabriel Scalliet.

Formal analysis: Diana Steinhauer, Marie Salat, Regula Frey, Andreas Mosbach, Torsten Luksch, Rasmus Hansen, Stephanie Widdison, Grace Logan, Robert A. Dietrich, Stephane Bieri, Stefano F. F. Torriani, Gabriel Scalliet.

Funding acquisition: Gabriel Scalliet.

Investigation: Diana Steinhauer, Marie Salat, Regula Frey, Andreas Mosbach, Torsten Luksch, Dirk Balmer, Rasmus Hansen, Grace Logan, Robert A. Dietrich, Stephane Bieri, Stefano F. F. Torriani, Gabriel Scalliet.

Methodology: Diana Steinhauer, Marie Salat, Andreas Mosbach, Torsten Luksch, Rasmus Hansen.

Project administration: Gabriel Scalliet.

Resources: Gert H. J. Kema, Helge Sierotzki, Stefano F. F. Torriani, Gabriel Scalliet.

Supervision: Gabriel Scalliet.

Validation: Rasmus Hansen.

Visualization: Andreas Mosbach, Torsten Luksch, Dirk Balmer, Stephanie Widdison, Grace Logan, Gabriel Scalliet.

Writing – original draft: Andreas Mosbach, Torsten Luksch, Rasmus Hansen, Robert A. Dietrich, Gabriel Scalliet.

Writing – review & editing: Andreas Mosbach, Stephanie Widdison, Robert A. Dietrich, Gabriel Scalliet.

References

1. Lamberth C, Jeanmart S, Luksch T, Plant A. Current challenges and trends in the discovery of agrochemicals. Science. 2013; 341(6147):742–6. Epub 2013/08/21. https://doi.org/10.1126/science.1237227 [pii]. PMID: 23950530

2. Horsefield R, Yankovskaya V, Sexton G, Whittingham W, Shiomi K, Omura S, et al. Structural and computational analysis of the quinone-binding site of complex II (succinate-ubiquinone oxidoreductase): a mechanism of electron transfer and proton conduction during ubiquinone reduction. Journal of Biological Chemistry. 2006; 281(11):7309–16. https://doi.org/10.1074/jbc.M508173200 PMID: 16407191

3. Zhu XL, Xiong L, Li H, Song XY, Liu JJ, Yang GF. Computational and experimental insight into the molecular mechanism of carboxamide inhibitors of succinate-ubquinone oxidoreductase. ChemMedChem. 2014; 9(7):1512–21. Epub 2014/03/29. https://doi.org/10.1002/cmdc.201300456 PMID: 24678033

4. Lancaster CR. Succinate:quinone oxidoreductases: an overview. Biochim Biophys Acta. 2002; 1553(1–2):1–6. Epub 2002/01/23. doi: S0005272801002407 [pii]. https://doi.org/10.1016/s0005-2728(01)00240-7 PMID: 11803013

5. Scalliet G, Boehler M, J. B, Geen PS, Kilby PM, Fonné-Pfister R. SDHIs and the Fungal Succinate Dehydrogenase. In: Dehne HW, Deising HB, Gisi U, Kuck KH, Russell PE, Lyr H, editors. Modern Fungicides and Antifungal Compounds VI; DPG-Verlag, Braunschweig, Germany 2011. p. 171–8.

6. Schmeling BV, Kulka M. Systemic fungicidal activity of 1,4-oxathiin derivatives. Science. 1966; 152 (3722):659–60. Epub 1966/04/29. doi: 152/3722/659 [pii] https://doi.org/10.1126/science.152.3722.659 PMID: 17779512

7. Snel M, Schmeling BV, Edgington LV. Fungitoxicity and structure-activity relationships of some oxathiin and thiazole derivatives. Phytopathology. 1970; 60:1164–9. https://doi.org/10.1094/phyto-60-1164 PMID: 5529696

8. Stammler G, Brix H-D, Glaettli A, Semar M, Schoefl U, editors. Biological properties of the carboxamide boscalid including recent studies on its mode of action. Proceedings, 16th International congress of Plant Protection; 2007; Glasgow.

9. FRAC. FRAC MoA Poster 2019-final FRAC web2019. Available from: http://www.frac.info/docs/default-source/publications/frac-mode-of-action-poster/frac-moa-poster-2019-final.pdf

10. Sierotzki H, Scalliet G. A review of current knowledge of resistance aspects for the next-generation succinate dehydrogenase inhibitor fungicides. Phytopathology. 2013; 103(9):880–7. Epub 2013/04/19. https://doi.org/10.1094/PHYTO-01-13-0009-RVW PMID: 23593940

11. Torriani SF, Melichar JP, Mills C, Pain N, Sierotzki H, Courbot M. Zymoseptoria tritici: A major threat to wheat production, integrated approaches to control. Fungal Genet Biol. 2015; 79:8–12. Epub 2015/06/21. https://doi.org/10.1016/j.fgb.2015.04.010 [pii]. PMID: 26092783

12. Skinner W, Bailey A, Renwick A, Keon J, Gurr S, Hargreaves J. A single amino-acid substitution in the iron-sulphur protein subunit of succinate dehydrogenase determines resistance to carboxin in Mycosphaerella graminicola. Curr Genet. 1998; 34(5):393–8. Epub 1998/12/31. https://doi.org/10.1007/s002940050412 PMID: 9871122

13. Fraaije BA, Bayon C, Atkins S, Cools HJ, Lucas JA, Fraaije MW. Risk assessment studies on succinate dehydrogenase inhibitors, the new weapons in the battle to control Septoria leaf blotch in wheat. Mol Plant Pathol. 2012; 13(3):263–75. Epub 2011/09/22. https://doi.org/10.1111/j.1364-3703.2011.00746.x PMID: 21933337

14. Scalliet G, Bowler J, Luksch T, Kirchhofer-Allan L, Steinhauer D, Ward K, et al. Mutagenesis and functional studies with succinate dehydrogenase inhibitors in the wheat pathogen Mycosphaerella graminicola. PLoS One. 2012; 7(4):e35429. Epub 2012/04/27. https://doi.org/10.1371/journal.pone.0035429 [pii]. PMID: 22536383; PubMed Central PMCID: PMC3334918.

15. Ishii H, Miyamoto T, Ushio S, Kakishima M. Lack of cross-resistance to a novel succinate dehydrogenase inhibitor, fluopyram, in highly boscalid-resistant isolates of *Corynespora cassiicola* and *Podosphaera xanthii*. Pest Management Science. 2011; 67(4):474–82. https://doi.org/10.1002/ps.2092 PMID: 21394880

16. Leroux P, Gredt M, Leroch M, Walker AS. Exploring mechanisms of resistance to respiratory inhibitors in field strains of *Botrytis cinerea*, the causal agent of gray mold. Applied & Environmental Microbiology. 2010; 76(19):6615–30. doi: 10.1128. PubMed PMID: AEM.00931-10.

17. Rehfus A, Strobel D, Bryson R, Stammler G. Mutations in sdh genes in field isolates of Zymoseptoria tritici and impact on the sensitivity to various succinate dehydrogenase inhibitors. Plant Pathology. 2018; 67(1):175–80. https://doi.org/10.1111/ppa.12715

18. Dooley H, Shaw MW, Spink J, Kildea S. The effect of succinate dehydrogenase inhibitor/azole mixtures on selection of Zymoseptoria tritici isolates with reduced sensitivity. Pest Manag Sci. 2016; 72(6):1150–9. Epub 2015/08/14. https://doi.org/10.1002/ps.4093 PMID: 26269125

19. FRAC. sdhi Fungicides working group 2019 [cited 2019]. Available from: http://www.frac.info/working-group/sdhi-fungicides

20. Klappach K, Zito R, Bryson R, Stammler G, Semar M, Mehl M, et al. Succinate Dehydrogenase Inhibitor (SDHI) Working Group 2019 [cited 2018]. Meeting on December 11/2, 2018, Protocol of the discussions and use recommendations of the SDHI Working Group of the Fungicide Resistance Action Committee (FRAC)]. Available from: http://www.frac.info/docs/default-source/sdhi-wg/sdhi-meeting-minutes/minutes-of-the-2018-sdhi-meeting-11-12th-of-december-2018-with-recommendations-for-2019.pdf

21. Yamashita M, Fraaije B. Non-target site SDHI resistance is present as standing genetic variation in field populations of Zymoseptoria tritici. Pest Manag Sci. 2018; 74(3):672–81. Epub 2017/10/13. https://doi.org/10.1002/ps.4761 PMID: 29024365; PubMed Central PMCID: PMC5814837.

22. Torriani SF, Brunner PC, McDonald BA, Sierotzki H. QoI resistance emerged independently at least 4 times in European populations of Mycosphaerella graminicola. Pest Manag Sci. 2009; 65(2):155–62. Epub 2008/10/04. https://doi.org/10.1002/ps.1662 PMID: 18833571

23. Kema GHJ, Mirzadi Gohari A, Aouini L, Gibriel HAY, Ware SB, van den Bosch F, et al. Stress and sexual reproduction affect the dynamics of the wheat pathogen effector AvrStb6 and strobilurin resistance. Nat Genet. 2018; 50(3):375–80. Epub 2018/02/13. https://doi.org/10.1038/s41588-018-0052-9 [pii]. PMID: 29434356

24. Fraaije BA, Cools HJ, Fountaine J, Lovell DJ, Motteram J, West JS, et al. Role of Ascospores in Further Spread of QoI-Resistant Cytochrome b Alleles (G143A) in Field Populations of Mycosphaerella graminicola. Phytopathology. 2005; 95(8):933–41. Epub 2008/10/24. https://doi.org/10.1094/PHYTO-95-0933 PMID: 18944416

25. Cools HJ, Fraaije BA. Update on mechanisms of azole resistance in Mycosphaerella graminicola and implications for future control. Pest Manag Sci. 2013; 69(2):150–5. Epub 2012/06/26. https://doi.org/10.1002/ps.3348 PMID: 22730104

26. Cools HJ, Mullins JG, Fraaije BA, Parker JE, Kelly DE, Lucas JA, et al. Impact of recently emerged sterol 14{alpha}-demethylase (CYP51) variants of Mycosphaerella graminicola on azole fungicide sensitivity. Appl Environ Microbiol. 2011; 77(11):3830–7. Epub 2011/04/12. https://doi.org/10.1128/AEM.00027-11 AEM.00027-11 [pii]. PMID: 21478305; PubMed Central PMCID: PMC3127603.

27. Cools HJ, Bayon C, Atkins S, Lucas JA, Fraaije BA. Overexpression of the sterol 14alpha-demethylase gene (MgCYP51) in Mycosphaerella graminicola isolates confers a novel azole fungicide sensitivity phenotype. Pest Manag Sci. 2012; 68(7):1034–40. Epub 2012/03/14. https://doi.org/10.1002/ps.3263 PMID: 22411894

28. Omrane S, Audeon C, Ignace A, Duplaix C, Aouini L, Kema G, et al. Plasticity of the MFS1 Promoter Leads to Multidrug Resistance in the Wheat Pathogen Zymoseptoria tritici. mSphere. 2017; 2(5). Epub 2017/11/01. doi: e00393-17 [pii] https://doi.org/10.1128/mSphere.00393-17 mSphere00393-17 [pii]. PMID: 29085913; PubMed Central PMCID: PMC5656749.

29. Omrane S, Sghyer H, Audeon C, Lanen C, Duplaix C, Walker AS, et al. Fungicide efflux and the MgMFS1 transporter contribute to the multidrug resistance phenotype in Zymoseptoria tritici field isolates. Environ Microbiol. 2015; 17(8):2805–23. Epub 2015/01/30. https://doi.org/10.1111/1462-2920.12781 PMID: 25627815

30. Roohparvar R, De Waard MA, Kema GH, Zwiers LH. MgMfs1, a major facilitator superfamily transporter from the fungal wheat pathogen Mycosphaerella graminicola, is a strong protectant against natural toxic compounds and fungicides. Fungal Genet Biol. 2007; 44(5):378–88. Epub 2006/11/17. doi: S1087-1845(06)00176-9 [pii] https://doi.org/10.1016/j.fgb.2006.09.007 PMID: 17107817

31. Roohparvar R, Mehrabi R, Van Nistelrooy JG, Zwiers LH, De Waard MA. The drug transporter MgMfs1 can modulate sensitivity of field strains of the fungal wheat pathogen Mycosphaerella graminicola to the strobilurin fungicide trifloxystrobin. Pest Manag Sci. 2008; 64(7):685–93. Epub 2008/03/28. https://doi.org/10.1002/ps.1569 PMID: 18366066

32. Gutierrez-Alonso O, Hawkins NJ, Cools HJ, Shaw MW, Fraaije BA. Dose-dependent selection drives lineage replacement during the experimental evolution of SDHI fungicide resistance in Zymoseptoria tritici. Evol Appl. 2017; 10(10):1055–66. Epub 2017/11/21. https://doi.org/10.1111/eva.12511 [pii]. PMID: 29151860; PubMed Central PMCID: PMC5680630.

33. Krishnan P, Meile L, Plissonneau C, Ma X, Hartmann FE, Croll D, et al. Transposable element insertions shape gene regulation and melanin production in a fungal pathogen of wheat. BMC Biol. 2018; 16(1):78. Epub 2018/07/18. https://doi.org/10.1186/s12915-018-0543-2 [pii]. PMID: 30012138; PubMed Central PMCID: PMC6047131.

34. Emanuelsson O, Nielsen H, Brunak S, von Heijne G. Predicting subcellular localization of proteins based on their N-terminal amino acid sequence. J Mol Biol. 2000; 300(4):1005–16. Epub 2000/07/13. https://doi.org/10.1006/jmbi.2000.3903 [pii]. PMID: 10891285

35. Grandaubert J, Bhattacharyya A, Stukenbrock EH. RNA-seq-Based Gene Annotation and Comparative Genomics of Four Fungal Grass Pathogens in the Genus Zymoseptoria Identify Novel Orphan Genes and Species-Specific Invasions of Transposable Elements. G3 (Bethesda). 2015; 5(7):1323–33. Epub 2015/04/29. https://doi.org/10.1534/g3.115.017731g3.115.017731 [pii]. PMID: 25917918; PubMed Central PMCID: PMC4502367.

36. Rudd JJ, Kanyuka K, Hassani-Pak K, Derbyshire M, Andongabo A, Devonshire J, et al. Transcriptome and metabolite profiling of the infection cycle of Zymoseptoria tritici on wheat reveals a biphasic interaction with plant immunity involving differential pathogen chromosomal contributions and a variation on the hemibiotrophic lifestyle definition. Plant Physiol. 2015; 167(3):1158–85. Epub 2015/01/18. https://doi.org/10.1104/pp.114.255927 [pii]. PMID: 25596183; PubMed Central PMCID: PMC4348787.

37. Fraaije BA, Bayon C, Atkins S, Cools HJ, Lucas JA, Fraaije MW. Risk assessment studies on succinate dehydrogenase inhibitors, the new weapons in the battle to control *Septoria* leaf blotch in wheat. Molecular Plant Pathology. 2011. Epub 20 SEP 2011. https://doi.org/10.1111/j.1364-3703.2011.00746.x PMID: 21933337

38. Plissonneau C, Hartmann FE, Croll D. Pangenome analyses of the wheat pathogen Zymoseptoria tritici reveal the structural basis of a highly plastic eukaryotic genome. BMC Biol. 2018; 16(1):5. Epub 2018/01/13. https://doi.org/10.1186/s12915-017-0457-4 [pii]. PMID: 29325559; PubMed Central PMCID: PMC5765654.

39. Hickman AB, Dyda F. DNA Transposition at Work. Chemical Reviews. 2016; 116(20):12758–84. https://doi.org/10.1021/acs.chemrev.6b00003 PMID: 27187082

40. Alvarez-Ponce D, Sabater-Muñoz B, Toft C, Ruiz-González MX, Fares MA. Essentiality Is a Strong Determinant of Protein Rates of Evolution during Mutation Accumulation Experiments in Escherichia coli. Genome Biology and Evolution. 2016; 8(9):2914–27. https://doi.org/10.1093/gbe/evw205 PMID: 27566759

41. Palma-Guerrero J, Torriani SF, Zala M, Carter D, Courbot M, Rudd JJ, et al. Comparative transcriptomic analyses of Zymoseptoria tritici strains show complex lifestyle transitions and intraspecific variability in transcription profiles. Mol Plant Pathol. 2016; 17(6):845–59. Epub 2015/11/27. https://doi.org/10.1111/mpp.12333 PMID: 26610174

42. Simões K, Hawlik A, Rehfus A, Gava F, Stammler G. First detection of a SDH variant with reduced SDHI sensitivity in Phakopsora pachyrhizi. Journal of Plant Diseases and Protection. 2018; 125(1):21–6. https://doi.org/10.1007/s41348-017-0117-5

43. Kupfer DM, Drabenstot SD, Buchanan KL, Lai H, Zhu H, Dyer DW, et al. Introns and splicing elements of five diverse fungi. Eukaryot Cell. 2004; 3(5):1088–100. Epub 2004/10/08. https://doi.org/10.1128/EC.3.5.1088-1100.2004 PMID: 15470237; PubMed Central PMCID: PMC522613.

44. Fouché S, Badet T, Oggenfuss U, Plissonneau C, Francisco CS, Croll D. Stress-driven transposable element de-repression dynamics in a fungal pathogen. bioRxiv. 2019:633693. https://doi.org/10.1101/633693

45. Mogi T, Kawakami T, Arai H, Igarashi Y, Matsushita K, Mori M, et al. Siccanin Rediscovered as a Species-Selective Succinate Dehydrogenase Inhibitor. The Journal of Biochemistry. 2009; 146(3):383–7. https://doi.org/10.1093/jb/mvp085 PMID: 19505951

46. Nose K, Endo A. Mode of action of the antibiotic siccanin on intact cells and mitochondria of Trichophyton mentagrophytes. J Bacteriol. 1971; 105(1):176–84. Epub 1971/01/01. PMID: 4250609; PubMed Central PMCID: PMC248339.

47. Miyadera H, Shiomi K, Ui H, Yamaguchi Y, Masuma R, Tomoda H, et al. Atpenins, potent and specific inhibitors of mitochondrial complex II (succinate-ubiquinone oxidoreductase). Proceedings of the National Academy of Sciences of the United States of America. 2003; 100(2):473–7. https://doi.org/10.1073/pnas.0237315100 PMID: 12515859

48. Moghaddam MB, Gross T, Becker A, Vilcinskas A, Rahnamaeian M. The selective antifungal activity of Drosophila melanogaster metchnikowin reflects the species-dependent inhibition of succinate-coenzyme Q reductase. Sci Rep. 2017; 7(1):8192. Epub 2017/08/16. https://doi.org/10.1038/s41598-017-08407-x [pii]. PMID: 28811531; PubMed Central PMCID: PMC5557811.

49. D'Costa VM, King CE, Kalan L, Morar M, Sung WW, Schwarz C, et al. Antibiotic resistance is ancient. Nature. 2011; 477(7365):457–61. Epub 2011/09/02. https://doi.org/10.1038/nature10388 [pii]. PMID: 21881561

50. Iwata F, Shinjyo N, Amino H, Sakamoto K, Islam MK, Tsuji N, et al. Change of subunit composition of mitochondrial complex II (succinate-ubiquinone reductase/quinol-fumarate reductase) in Ascaris suum during the migration in the experimental host. Parasitol Int. 2008; 57(1):54–61. Epub 2007/10/16. doi: S1383-5769(07)00103-1 [pii] https://doi.org/10.1016/j.parint.2007.08.002 PMID: 17933581

51. Roos MH, Tielens AG. Differential expression of two succinate dehydrogenase subunit-B genes and a transition in energy metabolism during the development of the parasitic nematode Haemonchus contortus. Mol Biochem Parasitol. 1994; 66(2):273–81. Epub 1994/08/01. doi: 0166-6851(94)90154-6 [pii]. https://doi.org/10.1016/0166-6851(94)90154-6 PMID: 7808477

52. Elorza A, Roschzttardtz H, Gomez I, Mouras A, Holuigue L, Araya A, et al. A nuclear gene for the iron-sulfur subunit of mitochondrial complex II is specifically expressed during Arabidopsis seed development and germination. Plant Cell Physiol. 2006; 47(1):14–21. Epub 2005/10/27. doi: pci218 [pii] https://doi.org/10.1093/pcp/pci218 PMID: 16249327

53. Szeto SS, Reinke SN, Oyedotun KS, Sykes BD, Lemire BD. Expression of Saccharomyces cerevisiae Sdh3p and Sdh4p paralogs results in catalytically active succinate dehydrogenase isoenzymes. J Biol Chem. 2012; 287(27):22509–20. Epub 2012/05/11. https://doi.org/10.1074/jbc.M112.344275 M112.344275 [pii]. PMID: 22573324; PubMed Central PMCID: PMC3391083.

54. Szeto SS, Reinke SN, Sykes BD, Lemire BD. Mutations in the Saccharomyces cerevisiae succinate dehydrogenase result in distinct metabolic phenotypes revealed through (1)H NMR-based metabolic footprinting. Journal of Proteome Research. 2010; 9(12):6729–39. https://doi.org/10.1021/pr100880y PMID: 20964315

55. Gebert N, Gebert M, Oeljeklaus S, von der Malsburg K, Stroud DA, Kulawiak B, et al. Dual function of Sdh3 in the respiratory chain and TIM22 protein translocase of the mitochondrial inner membrane. Mol Cell. 2011; 44(5):811–8. Epub 2011/12/14. https://doi.org/10.1016/j.molcel.2011.09.025 [pii]. PMID: 22152483

56. Brunner PC, Stefansson TS, Fountaine J, Richina V, McDonald BA. A Global Analysis of CYP51 Diversity and Azole Sensitivity in Rhynchosporium commune. Phytopathology. 2016; 106(4):355–61. Epub 2015/12/02. https://doi.org/10.1094/PHYTO-07-15-0158-R PMID: 26623995

57. Hawkins NJ, Cools HJ, Sierotzki H, Shaw MW, Knogge W, Kelly SL, et al. Paralog re-emergence: a novel, historically contingent mechanism in the evolution of antimicrobial resistance. Mol Biol Evol. 2014; 31(7):1793–802. Epub 2014/04/16. https://doi.org/10.1093/molbev/msu134 [pii]. PMID: 24732957; PubMed Central PMCID: PMC4069618.

58. Lendenmann MH, Croll D, McDonald BA. QTL mapping of fungicide sensitivity reveals novel genes and pleiotropy with melanization in the pathogen Zymoseptoria tritici. Fungal Genet Biol. 2015; 80:53–67. Epub 2015/05/17. https://doi.org/10.1016/j.fgb.2015.05.001 [pii]. PMID: 25979163

59. Bowler J, Scott E, Tailor R, Scalliet G, Ray J, Csukai M. New capabilities for Mycosphaerella graminicola research. Mol Plant Pathol. 2010; 11(5):691–704. Epub 2010/08/11. https://doi.org/10.1111/j.1364-3703.2010.00629.x [pii]. PMID: 20696006

60. Skinner W, Bailey A, Renwick A, Keon J, Gurr S, Hargreaves J. A single amino-acid substitution in the iron-sulphur protein subunit of succinate dehydrogenase determines resistance to carboxin in

Mycosphaerella graminicola. Current Genetics. 1998; 34(5):393–8. https://doi.org/10.1007/s002940050412 PMID: 9871122

61. Hellens R, Mullineaux P, Klee H. Technical Focus: a guide to Agrobacterium binary Ti vectors. Trends Plant Sci. 2000; 5(10):446–51. Epub 2000/10/25. doi: S1360-1385(00)01740-4 [pii]. https://doi.org/10.1016/s1360-1385(00)01740-4 PMID: 11044722

62. Hood EE, Gelvin SB, Melchers LS, Hoekema A. NewAgrobacterium helper plasmids for gene transfer to plants. Transgenic Research. 1993; 2(4):208–18. https://doi.org/10.1007/bf01977351

63. Waalwijk C, Mendes O, Verstappen EC, de Waard MA, Kema GH. Isolation and characterization of the mating-type idiomorphs from the wheat septoria leaf blotch fungus Mycosphaerella graminicola. Fungal Genet Biol. 2002; 35(3):277–86. Epub 2002/04/04. https://doi.org/10.1006/fgbi.2001.1322 [pii]. PMID: 11929216

64. Kema GHJ, Verstappen ECP, Todorova M, Waalwijk C. Successful crosses and molecular tetrad and progeny analyses demonstrate heterothallism in Mycosphaerella graminicola. Current Genetics. 1996; 30(3):251–8. https://doi.org/10.1007/s002940050129 PMID: 8753655

65. Wu TD, Nacu S. Fast and SNP-tolerant detection of complex variants and splicing in short reads. Bioinformatics. 2010; 26(7):873–81. Epub 2010/02/12. https://doi.org/10.1093/bioinformatics/btq057 PMID: 20147302; PubMed Central PMCID: PMC2844994.

66. Miller NA, Kingsmore SF, Farmer A, Langley RJ, Mudge J, Crow JA, et al. Management of High-Throughput DNA Sequencing Projects: Alpheus. J Comput Sci Syst Biol. 2008; 1:132. Epub 2008/12/26. https://doi.org/10.4172/jcsb.1000013 PMID: 20151039; PubMed Central PMCID: PMC2819532.

67. Vilella AJ, Severin J, Ureta-Vidal A, Heng L, Durbin R, Birney E. EnsemblCompara GeneTrees: Complete, duplication-aware phylogenetic trees in vertebrates. Genome Res. 2009; 19(2):327–35. Epub 2008/11/26. https://doi.org/10.1101/gr.073585.107 PMID: 19029536; PubMed Central PMCID: PMC2652215.

68. Sievers F, Wilm A, Dineen D, Gibson TJ, Karplus K, Li W, et al. Fast, scalable generation of high-quality protein multiple sequence alignments using Clustal Omega. Mol Syst Biol. 2011; 7:539. Epub 2011/10/13. https://doi.org/10.1038/msb.2011.75 PMID: 21988835; PubMed Central PMCID: PMC3261699.

69. Guindon S, Dufayard JF, Lefort V, Anisimova M, Hordijk W, Gascuel O. New algorithms and methods to estimate maximum-likelihood phylogenies: assessing the performance of PhyML 3.0. Syst Biol. 2010; 59(3):307–21. Epub 2010/06/09. https://doi.org/10.1093/sysbio/syq010 PMID: 20525638

70. Letunic I, Bork P. Interactive tree of life (iTOL) v3: an online tool for the display and annotation of phylogenetic and other trees. Nucleic Acids Res. 2016; 44(W1):W242–5. Epub 2016/04/21. https://doi.org/10.1093/nar/gkw290 PMID: 27095192; PubMed Central PMCID: PMC4987883.

71. Zarnack K, Maurer S, Kaffarnik F, Ladendorf O, Brachmann A, Kamper J, et al. Tetracycline-regulated gene expression in the pathogen Ustilago maydis. Fungal Genet Biol. 2006; 43(11):727–38. Epub 2006/07/18. doi: S1087-1845(06)00109-5 [pii] https://doi.org/10.1016/j.fgb.2006.05.006 PMID: 16843015

72. Bradford MM. A rapid and sensitive method for the quantitation of microgram quantities of protein utilizing the principle of protein-dye binding. Anal Biochem. 1976; 72:248–54. Epub 1976/05/07. doi: 0003-2697(76)90527-3 [pii]. https://doi.org/10.1006/abio.1976.9999 PMID: 942051

73. Shevchenko A, Tomas H, Havli J, Olsen JV, Mann M. In-gel digestion for mass spectrometric characterization of proteins and proteomes. Nature Protocols. 2007; 1:2856. https://doi.org/10.1038/nprot.2006.468 PMID: 17406544

74. Gerber PR, Muller K. MAB, a generally applicable molecular force field for structure modelling in medicinal chemistry. J Comput Aided Mol Des. 1995; 9(3):251–68. Epub 1995/06/01. https://doi.org/10.1007/bf00124456 PMID: 7561977

75. Cole JC, Korb O, McCabe P, Read MG, Taylor R. Knowledge-Based Conformer Generation Using the Cambridge Structural Database. Journal of Chemical Information and Modeling. 2018; 58(3):615–29. https://doi.org/10.1021/acs.jcim.7b00697 PMID: 29425456

76. Zhao Y, Truhlar DG. A new local density functional for main-group thermochemistry, transition metal bonding, thermochemical kinetics, and noncovalent interactions. The Journal of Chemical Physics. 2006; 125(19):194101. https://doi.org/10.1063/1.2370993 PMID: 17129083

77. Frisch MJ, Trucks GW, Schlegel HB, Scuseria GE, Robb MA, Cheeseman JR, et al. Gaussian 09 Revision A.02: Gaussian Inc. Wallingford CT 2009; 2009.